

Gravity anomalies and segmentation at the East Coast, USA continental margin

P. Wyer* and A. B. Watts

Department of Earth Sciences, University of Oxford, Parks Road, Oxford OX1 3PR, UK. E-mail: tony@earth.ox.ac.uk

Accepted 2006 May 11. Received 2006 May 3; in original form 2005 April 20

SUMMARY

The free-air gravity ‘edge effect’ anomaly at rifted continental margins has generally been attributed to the transition between thick continental and thin oceanic crust. While crustal thinning is a major contributor, recent studies suggest that sediment loading and magmatism may significantly modify the edge effect anomaly and cause it, at some margins, to be highly segmented along their strike. In this paper, we use a combined 3-D flexural backstripping and gravity anomaly modelling technique to determine the role that sediment loading has played in controlling the segmentation of Atlantic-type continental margins. We focus on the East Coast, USA since a substantial amount of high-quality seismic reflection and refraction, gravity, and magnetic data already exists for this margin. By calculating the gravity anomaly associated with rifting and sediment loading and iteratively comparing it to the observed free-air anomaly, we have determined the ‘best-fit’ elastic thickness, T_e , structure of the margin. We show that $0 < T_e < 40$ km and that T_e varies across-strike and along-strike the margin. Since T_e is a proxy for the long-term ($> 10^5$ a) integrated strength of the lithosphere, these results imply that weak regions abut strong ones at the East Coast, USA margin. T_e generally decreases with increase in the amounts of crustal thinning, β , and the flexed basement curvature, K , suggesting it is controlled, at least in part, by the mechanical structure of the pre-rift lithosphere and yielding due to flexural loading. However, there is considerable scatter, suggesting other factors such as along-strike changes in crustal composition. Irrespective, we show that an isostatic anomaly that takes into account the ‘best-fit’ T_e distribution is significantly reduced in spectral power compared with one which is computed assuming only Airy compensation (i.e. $T_e = 0$ km). This is not to imply that rifting and sediment loading completely accounts for the anomalies along-strike and across-strike the East Coast, USA margin. To the contrary, significant isostatic anomaly highs and lows persist, especially in inner and middle shelf regions. One of the most prominent is an arcuate, 670 km long, high with flanking lows offshore Carolina that we attribute to magmatism during the initial stages of continental break-up.

Key words: East Coast USA, flexure, gravity anomalies, isostasy, rifted margins, sediment thickness.

1 INTRODUCTION

The free-air gravity anomaly ‘edge effect’ at rifted continental margins has traditionally been explained as the consequence of the transition between thick continental crust and thin oceanic crust. Worzel (1965), for example, showed that when an Airy model of isostasy is used to describe the thinning, there is a gravity anomaly ‘high’ over the thick crust and a ‘low’ over the flanking thin crust. Such a

high–low ‘couple’ is a distinctive feature of rifted margins where it extends more or less uninterrupted along their strike. Furthermore, seismic refraction data (e.g. Keen *et al.* 1975) shows that the Moho at many rifted margins is approximately in the position that would be predicted by an Airy model in which continental shelf, slope and rise are compensated at depth by variations in the thickness of a uniform density crust.

The success of the Airy model led a number of workers to calculate isostatic anomalies in an attempt to reveal other, non-isostatic, sources at rifted margins. Talwani & Eldholm (1973), for example, used an Airy isostatic anomaly (i.e. one calculated by subtracting the gravity effect of the topography and its Airy-type compensation from the free-air anomaly) to show that many margins in the Atlantic

*Present address: MARGINS Office, Dept. of Earth and Planetary Sciences, Washington University, St. Louis, MO 63130, USA.

and Indian Oceans are associated with an 'outer gravity high', the steep landward edge of which they attributed to density differences in the region of the ocean–continent boundary (OCB).

Walcott (1972) and Gunn (1944) before him, showed that sediment loading could also contribute significantly to the edge effect anomaly. Walcott (1972) showed, for example, that in the case of the Mississippi river delta, the amplitude and wavelength of the edge effect anomaly associated with the initial rifting may be substantially modified by sediment loading, depending on the flexural rigidity and equivalent elastic thickness, T_e , structure of the margin.

Rabinowitz & LaBreque (1979), however, found a poor correlation between the peak of the outer isostatic anomaly high and the maximum sediment thickness. They concluded that sediment loading was not a major contributor. In support of this conclusion, Rabinowitz & LaBreque (1979) calculated a sediment-corrected isostatic anomaly (i.e. a free-air anomaly that is corrected for the isostatic compensation of topography and sediments) and showed that and 'outer high' was still present. They attributed the high to elevated, partially compensated, oceanic crust that abuts continental crust.

A difficulty with the Rabinowitz & LaBreque (1979) study is that they assumed an Airy rather than a flexure model for the compensation of the sediments. Karner & Watts (1982) showed that some of the isostatic anomaly highs of Rabinowitz & LaBreque (1979) could, instead, be explained by flexural loading. In particular, they showed that sediment loading is associated with an Airy isostatic anomaly high that was bounded on one side by a steep gradient and on the other by a gently decreasing 'tail'. The anomaly closely replicated the observed one.

Watts (1988) developed a combined backstripping and gravity modelling technique that allowed the role of flexure at rifted margins to be quantitatively determined directly from sediment thickness and gravity anomaly data. By calculating the 'sum' anomaly due to the combined effects of rifting and sediment loading and comparing it to the free-air gravity anomaly at the East Coast, USA margin in the region of the Baltimore Canyon Trough, he argued that little material has been added to the continental crust following rifting. Moreover, Watts (1988) demonstrated that T_e of extended continental lithosphere is relatively low (compared to unstretched and oceanic lithosphere) and ~ 5 km. The technique has subsequently been applied to other rifted margins, notably Mozambique (Watts 2001a), Gabon and Cabinda (Watts & Stewart 1998), Namibia (Stewart *et al.* 2000), the Madagascar–Western India conjugate pair (Chand & Subrahmanyam 2003), and Eastern India (Krishna *et al.* 2000) where it has provided useful information not only on T_e , but also the structure of rifted crust and mantle, the along-strike segmentation, the OCB, and the role of flexure during and following rifting.

The question of segmentation is of particular interest since it may reflect the influence on rifted continental lithosphere of a mid-oceanic ridge during the early stages of rifting. Behn & Lin (2000), for example, used the satellite-derived gravity field of Sandwell & Smith (1997) and a sediment thickness grid compiled by the USGS (Klitgord *et al.* 1994; Hutchinson *et al.* 1996) to calculate a sediment-corrected isostatic anomaly at the East Coast, US margin. They showed that isostatic anomalies in the region of the shelf break were highly segmented along-strike the margin and that they are of amplitude ± 30 mGal and wavelength, λ , of 100 km and 300–500 km. The former is comparable to the wavelength of the gravity segmentation at mid-oceanic ridges (Sempere *et al.* 1990), suggesting a link between them. Furthermore, Behn & Lin (2000) noted that two minima in the isostatic anomaly high approximately corre-

sponded to the early traces of the Kane and Atlantis fracture zones, suggesting that they may define boundaries of a single 'tectonic corridor' in the North Atlantic.

The analysis of Behn & Lin (2000) was, like the earlier study of Rabinowitz & LaBreque (1979) limited to an Airy-type model. Behn & Lin (2000) recognized this limitation, suggesting that while their Airy isostatic anomalies correlated with certain fracture zone defined 'tectonic corridors', their cause may also be a combination of variations in the flexural strength of the lithosphere and the amount of thickened igneous crust along-strike the margin.

In this paper, we use a combined 3-D flexural backstripping and gravity anomaly modelling technique to determine the role that sediment loading has played in controlling the segmentation observed along-strike and across-strike the East Coast, USA rifted margin. By calculating the gravity anomalies expected for rifting and sediment loading and iteratively comparing their sum to observed free-air gravity anomalies, we have determined the T_e structure and, hence, the sediment-corrected flexural isostatic anomaly along the margin. We show that the flexural isostatic anomaly is significantly reduced in amplitude compared to anomalies computed assuming an Airy model. Despite this, some flexural isostatic anomalies persist both along-strike and across-strike the margin and we attribute one of them, a 670-km-long arcuate high offshore Virginia and Carolina, to the effects of magmatism during the initial stages of rifting.

2 GEOLOGICAL SETTING

The East Coast, USA continental margin formed following the rifting apart of the Pangea 'super continent' and the opening of the Central Atlantic ocean during the Late Triassic and Early Jurassic. The margin is characterized by up to about 15 km of gently dipping Mesozoic to Tertiary sediments that overlie a much older Precambrian and Palaeozoic basement. Sediment thickness varies along-strike and across-strike the shelf such that depressions with thick sediments (Schlee 1981) are separated by platforms with thinner sediments. Together, the depressions and platforms give the shelf a distinct structural segmentation, a point recognized by Brown *et al.* (1972) who referred to them as embayments and arches, respectively.

Seismic reflection profile data reveal both syn-rift and post-rift sedimentary sequences (Grow 1981). The syn-rift is found onshore in narrow fault-bounded grabens (e.g. Newark, Connecticut and Culpepper) (Manspeizer 1985). The grabens contain upwards of 5 km of fanglomerates, flood plain and lacustrine deposits of Late Triassic to Early Jurassic age. Similar features are difficult to recognize offshore, but south of Long Island there are grabens that are unconformably overlain by a thick post-rift, the bulk of which is believed to be of Jurassic age (Hutchinson *et al.* 1986). The post-rift reaches its maximum thickness beneath the outer shelf and slope, but it extends onshore where it forms part of the East Coast, USA coastal plain. The coastal plain sediments, which are Cretaceous and Cenozoic in age, 'pinch-out' at the fall-line. The Jurassic does not outcrop in the coastal plain and has only been recovered in a few deep wells at the coast.

In the mid-1970s, the margin was the target of deep stratigraphic test drilling (Schlee *et al.* 1976). Backstripping of biostratigraphic data from the COST B-2 test well offshore New Jersey shows a Total Tectonic Subsidence (TTS) of ~ 1.5 km. Moreover, the subsidence decreases exponentially through time, from fast initially to slow later on (Steckler & Watts 1978). When an additional horizon top is added

to the biostratigraphic data that takes into account the thickness of the post-rift *beneath* the well, then the TTS increases to ~ 5.2 km. Watts & Marr (1995) showed that the TTS could be explained by an instantaneous rifting model (McKenzie 1978) with a stretching factor, β , of 2.4 to 4.4, the range reflecting uncertainties in the water depth of deposition and the magnitude of sea level through time. The β range implies a crustal thickness of 7.1–13.0 km beneath the well, assuming an unstretched, zero-elevation, crustal thickness of 31.2 km.

Wide-angle seismic refraction data (LASE study group 1986) show that the crust is thin beneath the COST B-2 well and has a thickness that is in general accord with predictions based on backstripping. Moreover, the data show that the thinned crust has high lower crustal velocities (7.2–7.5 km s⁻¹), compared to that of adjacent oceanic crust. Trehu *et al.* (1989) offshore North Carolina and Holbrook *et al.* (1994a) offshore Virginia noted similar high velocities, which they attributed to magmatic material that ‘ponds’ beneath extended continental crust during or following rifting.

Based on these and other studies, Holbrook & Kelemen (1993) concluded that the East Coast, USA margin is underlain by a thickness of up to 25 km of magmatic material which extends for >1000 km along-strike the margin. Offshore Virginia, the magmatic material is associated with seaward-dipping reflectors (SDRs) that have been attributed to subaerial extrusive volcanism followed by subsidence and rotation of the underlying rifted crust. Subsequently, McHone (2000) speculated that magmatic material in the form of SDRs extending along the margin from offshore Nova Scotia to Florida and it has been suggested (Marzoli *et al.* 1999) that the entire East Coast, USA is a volcanic-type margin which formed part of a Late Triassic/Early Jurassic Central Atlantic Magmatic Province (CAMP).

3 DATA SOURCES

3.1 Bathymetry and gravity

The bathymetry and gravity data used in this paper are based mainly on the Decade of North American Geology (DNAG) data set, as released by the National Geophysical Data Center in 1989. The bathymetry was compiled from United States Geological Survey (USGS), Defense Mapping Agency (DMA), National Geodetic Survey (NGS) and National Geophysical Data Center (NGDC) data. The gravity data was compiled by the DMA and comprises academic, government, and industry survey data.

The gravity anomaly and bathymetry data were provided by DNAG as a 4 × 4 km Transverse Mercator grid. We converted the grid to 2.5 × 2.5 min ‘bins’ and then gridded it at a 5 × 5 min interval using the Generic Mapping Tools (GMT) program surface (Wessel & Smith 1991) with a tension, T , of 0.25 and 0.35 for the gravity and bathymetry, respectively.

Fig. 1 shows a bathymetry, sediment thickness, and gravity anomaly map of the East Coast, USA margin. The bathymetry data is as provided by DNAG. The gravity data (free-air anomaly offshore, Bouguer anomaly onshore) is also as provided by DNAG, except that a satellite-derived field, up to harmonic degree and order 16 (Rapp & Pavlis 1990), has been removed from it. We chose this field because it is dominated by the gravity anomaly low associated with late-glacial rebound in North America and, hence, is representative of deep processes that are unrelated to the crustal structure of the East Coast, USA margin.

3.2 Sediment thickness

The sediment thickness data is based on the compilations of USGS (Hutchinson, personal communication, 2002), COSUNA (Childs & Salvador 1985), Mountain & Tucholke (1985), and Laske & Masters (1997).

The USGS compilation is based on >30 000 line km of multichannel seismic reflection acquired in the 1970s. The data were re-processed in the 1990s and prominent reflectors have been dated using well-ties and other direct sample data. A total of 19 stratigraphic units have been mapped (Fig. 2) and depth converted using interval (i.e. stacking) velocities derived from the reflection data, as described in Hutchinson *et al.* (1996). We received the data as a 5 × 5 min grid of depth to individual horizon tops (Hutchinson personal communication).

The COSUNA compilation is mainly based on onshore well data and provides information on depths to individual horizon tops. The digital data contains >18 000 records, but its utility is limited by the low resolution of some of the well locations. Despite this, we found the derived sediment thickness distribution to be consistent with that mapped by Brown *et al.* (1972) in the region of the coastal plain.

The Mountain & Tucholke (1985) sediment contour maps are based on the USGS multichannel data as well as a number of other single-channel and multichannel seismic reflection profile data over the continental slope and rise.

Finally, the Laske & Masters (1997) data set is a 1 × 1° grid of onshore and offshore total sediment thickness. This comprises mainly Exxon data onshore and the published literature offshore.

We have combined the USGS, COSUNA, Laske & Masters (1997) and Mountain & Tucholke (1985) data sets into a single 5 × 5 min grid that comprises 7 individual isopachs (Fig. 2). Within the region of USGS data coverage, the isopachs are as defined by the depth converted seismic data. Outside of this area, interpolation (using GMT surface) was carried out. The ocean age file of Muller *et al.* (1997) was used to map the seaward ‘pinch-out’ of some isopachs.

Fig. 3 compares the depths to stratigraphic horizons based only on the USGS grid (left-hand side column) to that based on our combined grid (right-hand side column). The figure shows that the combined grid is representative of the USGS data, outlining well the stratigraphic ‘architecture’ of the shelf basins and their extensions onshore and to beneath the slope and rise.

4 METHODOLOGY

We have analysed the combined sediment thickness grid using a process-oriented 3-D combined backstripping and gravity modelling technique (Fig. 4). The main computational steps in process-oriented modelling have been previously discussed by Watts (1988) and, more recently, by Stewart *et al.* (2000) and Watts (2001a) and so will only be briefly outlined here. Firstly, a sediment grid is flexurally backstripped in order to determine the TTS and, hence, the crustal structure at the time of rifting. Secondly, the restored rift structure is used to calculate the gravity anomalies associated with rifting and sedimentation, assuming these processes to have been the main ones that were operative during margin evolution. The final step is to compare the sum of the calculated gravity effect of rifting and sedimentation to the observed free-air gravity anomaly.

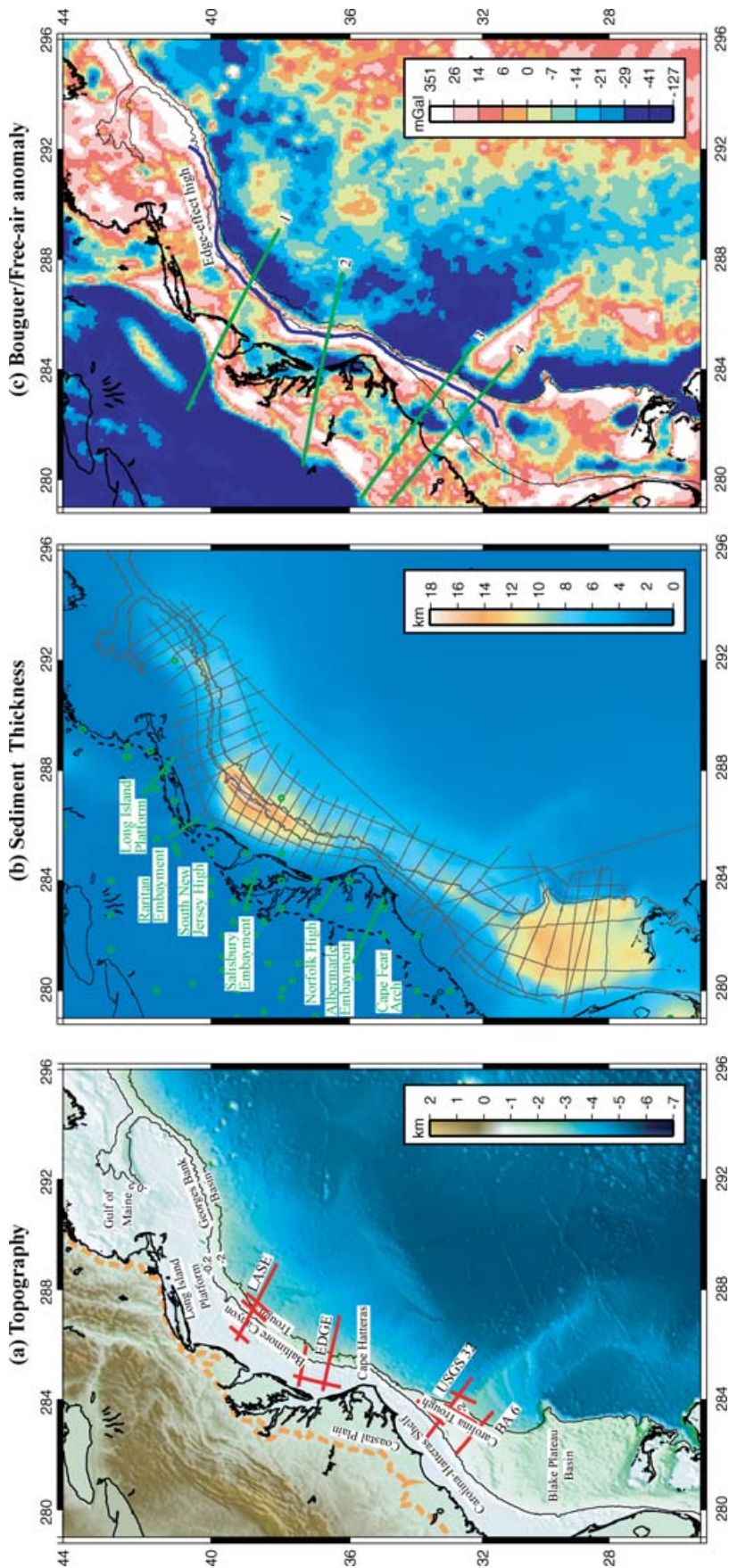


Figure 1. Location map of the East Coast, USA continental margin. (a) Topography based on a 2.5×2.5 min grid of Decade of North American Geology (DNAG) data. Solid lines show the location of the LASE (LASE study group 1986), EDGE-801 (Holbrook *et al.* 1994a), USGS-32 (Trehu *et al.* 1989) and BA-6 (Holbrook *et al.* 1994b) seismic refraction profiles. (b) Sediment thickness based on the compilations of USGS (Klitgord *et al.* 1994) (Hutchinson *et al.* 1996), COSUNA (Childs & Salvador 1985) and Mountain & Tucholke (1985). Solid lines—1973–1978 multichannel seismic reflection profiles used in the USGS compilation. Circles—boreholes used in the COSUNA compilation. Thick dashed line = Fall line. (c) Gravity anomaly (free-air—offshore; Bouguer—onshore) based on a 2.5×2.5 min grid of DNAG data. The gravity anomaly has had a long-wavelength satellite derived degree and order 16 field removed from it. Solid lines show Profiles 1–4 (Fig. 7).

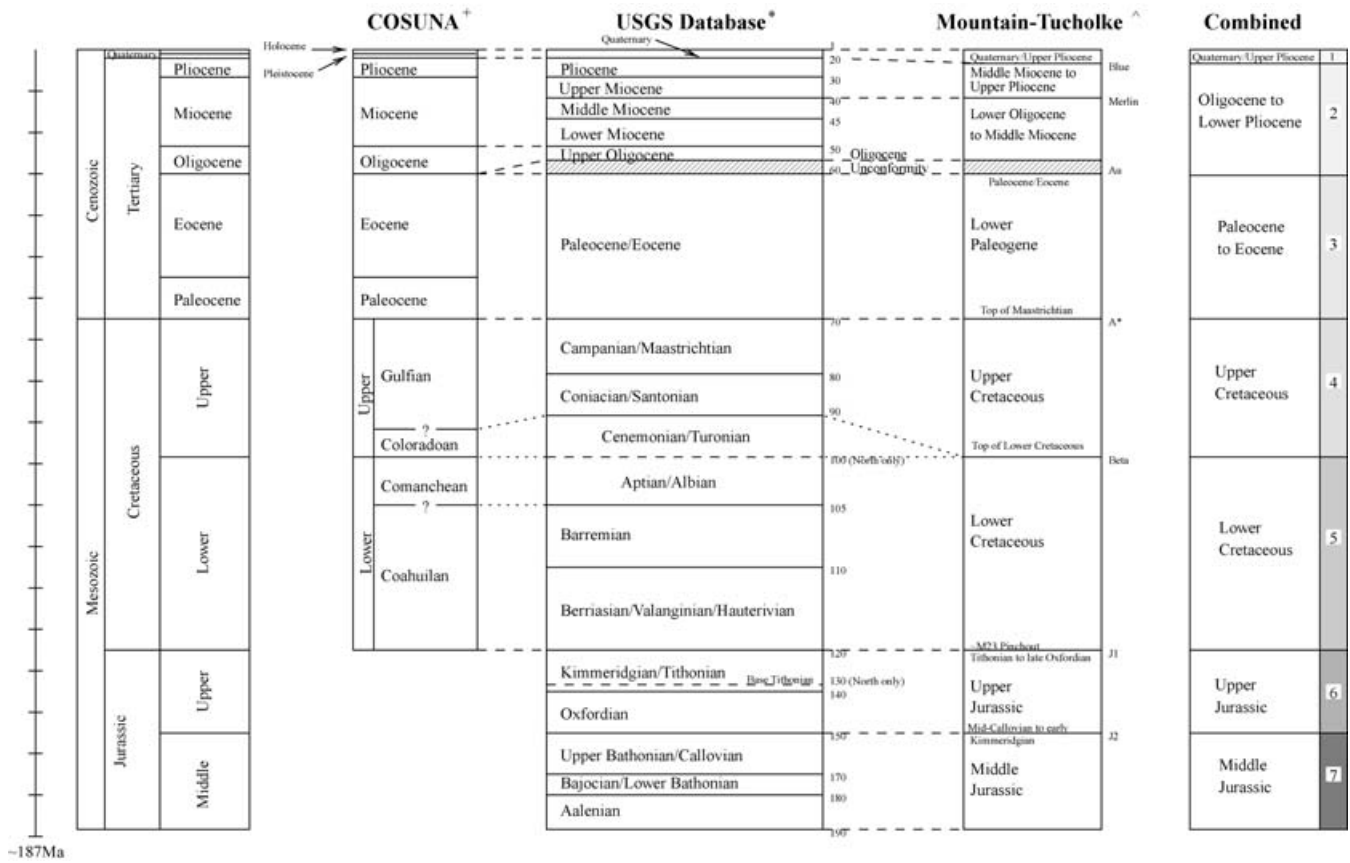


Figure 2. Stratigraphic correlations used in COSUNA (Childs & Salvador 1985), the USGS (Klitgord *et al.* 1994; Hutchinson *et al.* 1996) and Mountain & Tucholke (1985) and this paper. The COSUNA correlation is based on well and outcrop data while the USGS and Mountain & Tucholke (1985) correlations are based on seismic stratigraphy. The number to the right of the USGS database column indicates the approximate age (Ma). The combined column indicates the stratigraphic divisions and unit numbers assumed in this paper.

4.1 Flexural backstripping

We have flexurally backstripped the sediments using both uniform and spatial variations in T_e and with T_e distributions that are both constant and varying through time.

Spatially variable T_e

Spectral studies of topography and gravity anomaly data suggest that continental T_e ranges from a few km to >70 km and that it varies spatially over relatively short (~100 km) horizontal scales (e.g. Wang & Mareschal 1999). We have, therefore, used 3-D finite difference techniques (e.g. Van Wees & Cloetingh 1994) to investigate the possibility that T_e may vary across-strike and along-strike the East Coast, USA margin.

The differential equation for bending of a vertically loaded thin elastic plate of variable thickness and infinite extent is given by (e.g. Timoshenko & Woinowsky-Krieger 1959):

$$\begin{aligned}
 D \nabla \nabla w + 2 \frac{\partial D}{\partial x} \frac{\partial}{\partial x} \nabla w + 2 \frac{\partial D}{\partial y} \frac{\partial}{\partial y} \nabla w + \nabla D \nabla w \\
 - (1 - \nu) \left\{ \frac{\partial^2 D}{\partial x^2} \frac{\partial^2 w}{\partial y^2} - 2 \frac{\partial^2 D}{\partial x \partial y} \frac{\partial^2 w}{\partial x \partial y} + \frac{\partial^2 D}{\partial y^2} \frac{\partial^2 w}{\partial x^2} \right\} \\
 + \rho_1 g w = \rho_2 g h,
 \end{aligned}
 \tag{1}$$

where w = flexure, D = flexural rigidity, ν = Poisson's ratio, ρ_1 = the density difference between the substrate and material infilling

the flexure, ρ_2 = the density difference between the load and the material that it displaces, g = gravity, and h = normal load height.

$$\nabla = \frac{\partial^2}{\partial y^2} + \frac{\partial^2}{\partial x^2}$$

The rigidity derivatives in eq. (1) are obtained by differentiation of the T_e distribution in the Fourier domain. These are then converted to derivatives of the rigidity using differential terms of:

$$D = \frac{E T_e^3}{12(1 - \nu^2)}$$

where E = Young's modulus. For example,

$$\frac{\partial^2 D}{\partial x \partial y} = \frac{\partial D}{\partial T_e} \left(\frac{\partial^2 T_e}{\partial x \partial y} \right) = \frac{E T_e^2}{4(1 - \nu)} \left(\frac{\partial^2 T_e}{\partial x \partial y} \right) = \frac{3D}{T_e} \left(\frac{\partial^2 T_e}{\partial x \partial y} \right)$$

Evaluation of the derivatives in eq. (1) can be approximated by direct substitution of centred finite difference terms as described by Gahli & Neville (1989).

A detailed description of our technique (together with a complete listing of the derivatives) is given in Wyer (2003) and so will only be briefly outlined here. Basically, we use a Taylor series expansion up to the first Δx and Δy term to approximate the first and second-order derivatives in x and y of the flexure $w(x, y)$. Higher-order derivatives are similarly approximated by expansion in terms of the second-order derivatives up to the first Δx and Δy terms.

We have compared the flexure computed using the finite difference approximation to the analytical uniform plate solutions for

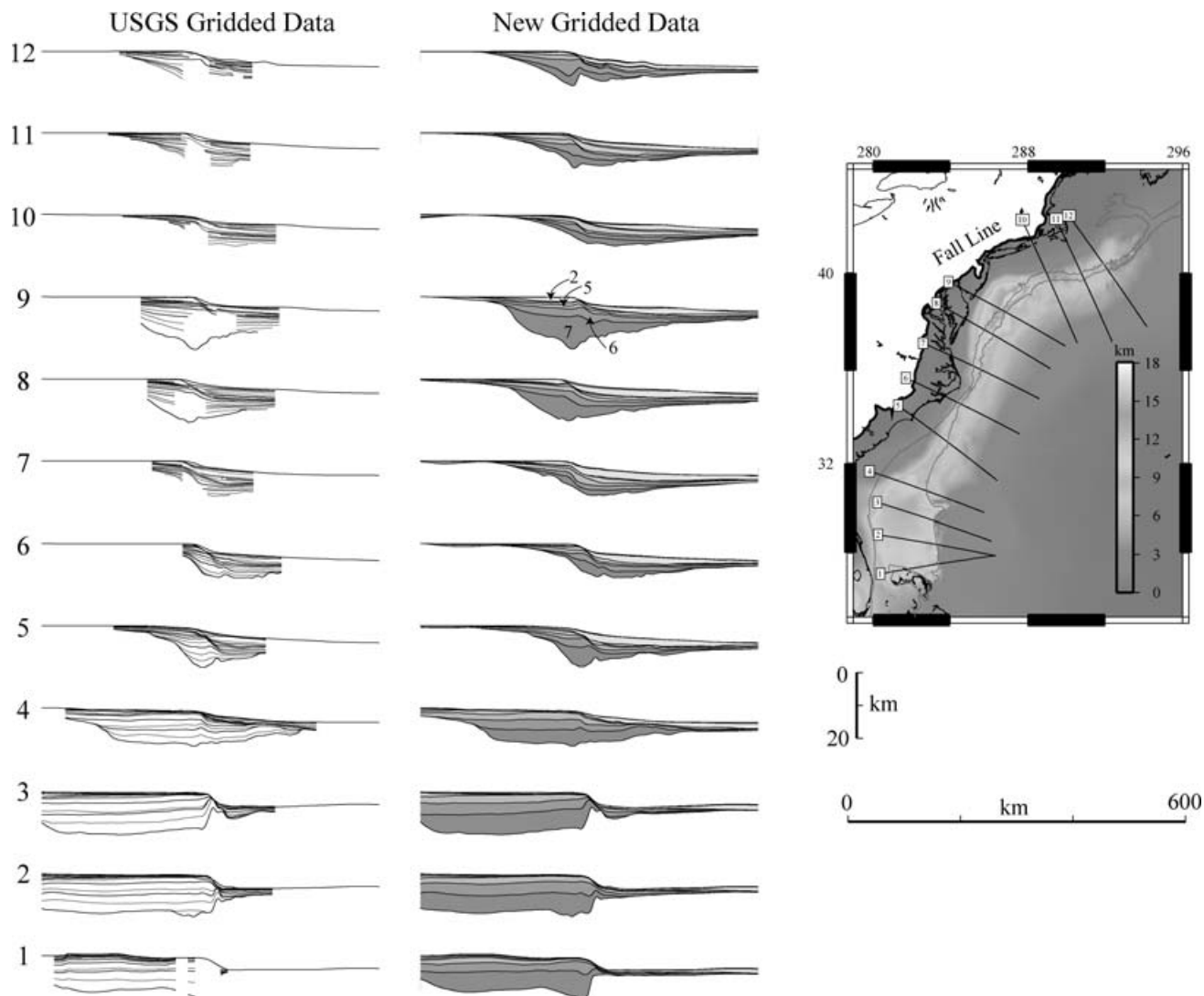


Figure 3. Seismic stratigraphy along 12 representative profiles of the East Coast, USA continental margin. (a) Depths to digitized reflectors in the USGS database. Reflector terminations indicate no data. Shading as in the combined column in Fig. 2. (b) Stratigraphic units 1–7 constructed from the COSUNA, USGS and Mountain & Tucholke (1985) data sets. Inset map shows location of profiles and total sediment thickness.

disc-shaped loads of Brotchie & Silvester (1969). We found a close agreement for a range of sizes of discs. Typically, maximum differences between the two different approaches are <2 per cent of the flexure, with a rms misfit of ~ 0.5 per cent.

Temporal variable T_e

Oceanic flexure studies suggest that T_e depends on both plate and load age (e.g. Watts & Zhong 2000). Submarine volcanoes that form on a mid-oceanic ridge, for example, are associated with low values ($2 < T_e < 10$ km) while similar-size features that form off-ridge correlate with high values ($25 < T_e < 30$ km). T_e is described well by the depth to the 300–600°C isotherms based on the thermal cooling plate model and is given approximately by $3.0 \times t^{1/2}$ where t is the age of the oceanic lithosphere at the time of loading.

We do not presently know whether continental T_e depends in the same way on plate and load age as oceanic lithosphere. The problem is that there is a wide range of continental T_e estimates and no single set of thermal parameters (e.g. thermal thickness) can explain the distribution of all the data (Watts 2001b).

Most T_e estimates at rifted continental margins represent the average response of the underlying basement to sediment loading. There is evidence, however, from margins that have been *discretely* loaded of a T_e that may increase with age. For example, T_e is low (~ 13 km) at the South China Sea margin which rifted during Palaeocene–Eocene and was loaded by orogenic (e.g. thrust/fold) loads in Taiwan during the Pliocene (Lin & Watts 2002) and is high (~ 30 km) at the Eastern India margin which is Late Cretaceous and was loaded by the Bengal deep-sea fan during the mid-Tertiary (Krishna *et al.* 2000).

We have, therefore, included in our analysis of the East Coast, USA margin the possibility that T_e may increase with age since rifting.

Compaction

The effects of compaction are of importance, especially in the way that it influences the sediment density and, hence, magnitude of the loads that have been applied through geological time.

We have assumed an Athy-type porosity versus depth function (Athy 1930) with a grain density, ρ_g , of 2720 kg m $^{-3}$, a surface

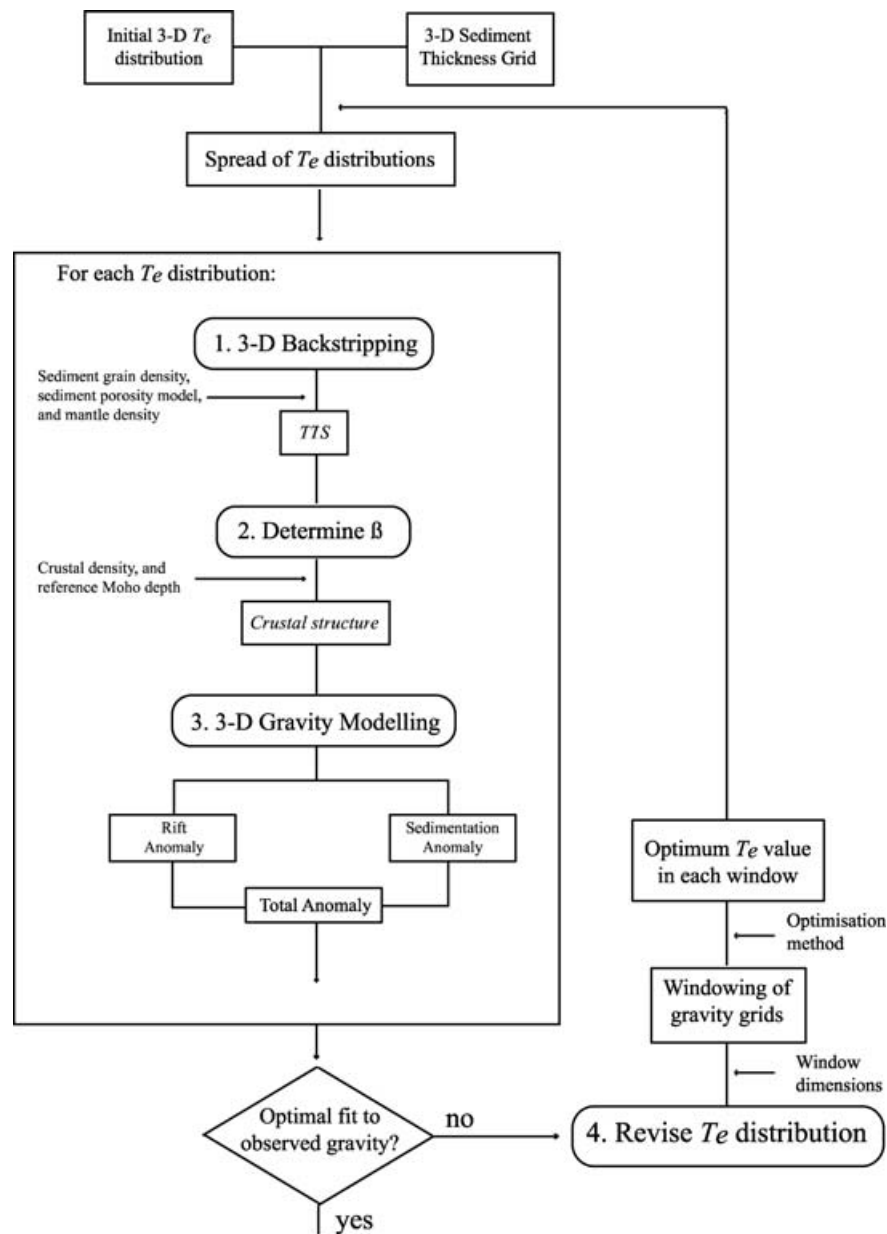


Figure 4. Flow diagram showing how flexural backstripping and gravity modelling are used iteratively to determine the spatial distribution of T_e associated with sediment loading. The input is a sediment thickness, gravity anomaly, and an initial T_e grid. The output is a spatial varying T_e grid, which is obtained by modifying the initial T_e distribution until it provides the best-fit between the observed and calculated free-air gravity anomaly.

porosity, $\phi_0 = 0.15$, and a depth constant, $Z = 4629$ m. The grain density is typical of sands. The two other parameters imply 2467 kg m^{-3} for the density of the uppermost layer and 2720 kg m^{-3} for the lowermost layer in the thickest part of the margin. Data at the COST B-2 well in the outer shelf suggest higher ϕ_0 and lower Z values (e.g. Steckler & Watts 1978). However, we found that parameter pairs which are more consistent with the COST B-2 data (e.g. $\phi_0 = 0.55$ and $Z = 3000$ m) converge rapidly to similar bulk densities at depth and that they, therefore, had little effect on the overall sediment load and, hence, the resulting gravity anomaly.

We recognize, of course, that such a compaction model oversimplifies the density structure of the sediments. This is because facies changes result in densities that vary both across-strike and along-strike the margin. As pointed out by Behn & Lin (2000), however, the isostatic gravity anomaly, is relatively insensitive to

moderate changes in sediment grain density. Moreover, lateral density anomalies within a sedimentary unit are unlikely to produce gravity anomalies of the amplitude and wavelength associated with the flexural loading. We do find, however, significant discrepancies in the gravity anomaly if compaction is ignored. The reason for this is that the load may be greatly under-estimated in areas of thick sediment and over-estimated in areas of thin sediment.

4.2 Restoration of the crustal structure at the time of rifting

We have used the sediment backstrip to restore the crustal structure at the time of rifting assuming both Airy and flexural-type isostatic models.

Airy

The Airy model assumes a state of local isostasy during rifting. The amount of crustal thinning (i.e. the stretching factor, β) is computed from the backstrip (i.e. the water-filled *TTS*) assuming:

$$\beta = \frac{(\rho_m - \rho_c)T_c}{(\rho_m - \rho_c)T_c - TTS(\rho_m - \rho_w)}, \quad (2)$$

where T_c = initial crustal thickness, and ρ_c , ρ_m and ρ_w are the densities of the crust, mantle and water, respectively.

Thermal models suggest that eq. (2) can be used to predict β , provided the appropriate choice is made concerning ρ_c , ρ_m and ρ_w . We assumed here densities of 2850, 3330 and 1030 kg m⁻³, respectively. This choice of densities, as Watts (2001b, fig. 7.22) has shown predicts well the correct relationship between β and *TTS* for a 180 Myr margin.

Flexure

The flexure model takes into account the possibility that margin lithosphere is of finite strength during rifting. The strength could either enhance or limit extension and might create an isostatic imbalance that will result in a different crustal structure than that predicted by an Airy model. Kooi *et al.* (1992) and Weissel & Karner (1989) have formulated models in which the amount of extension depends on a parameter they dub, the depth of necking, Z_{neck} . While Kooi *et al.* (1992) consider Z_{neck} the depth to a strength maxima, Weissel & Karner (1989) regard it as the depth to a detachment surface. Irrespective, the Z_{neck} concept allows the possibility of T_e during rifting to be modelled as has been demonstrated by Kooi *et al.* (1992) for the Gulf of Lyon, Watts & Stewart (1998) for the Gabon and Cabinda, and Keen & Dehler (1997) for the Canada and southwest Greenland margins.

We have calculated the sum gravity anomaly for a wide range of Z_{neck} and T_e and compared it to the observed free-air gravity anomaly on four profiles of the East Coast, USA margin. We found that the best-fit Z_{neck} was generally close to the 7.9 km depth at which extension with our density parameters produces no net isostatic imbalance, and hence an apparent Airy-type rift crustal structure. We recognize that T_e during rifting might be significant. We found, however, that irrespective of the T_e assumed in the backstripping, the combination of a very shallow or very deep Z_{neck} and high T_e was unable to adequately explain the amplitude and wavelength of the observed edge effect anomaly. We, therefore, conclude that the assumption of an Airy model during rifting is a reasonable one that is compatible with the data.

4.3 Gravity anomaly modelling

We calculated the gravity anomalies of the restored crustal structure (i.e. the rifting anomaly) and sedimentation (i.e. the sedimentation anomaly) using a 2-D version of Parker's Fast Fourier Transform method with the number of terms, n , of 4 (Parker 1972).

In the process-oriented technique, the sum anomaly is calculated by adding the rift and sedimentation anomalies (Watts 1988). The rift anomaly is obtained by backstripping and calculating the gravity effect of the water-filled basin above the backstrip and the mantle below the backstrip Moho (2 bodies). The sedimentation anomaly is then calculated from the sediment load (1 body), which extends above the backstrip, and its compensation. The compensation arises from the sediment 'infill' between the backstrip and the basement

(1 body) and the crust between the backstrip and flexed Moho (1 body). Together, this yields a total of five bodies.

We found that when repeatedly applied to gridded data sets, the technique of Watts (1988) was too computer intensive. The main problem was in the calculation of the sedimentation anomaly where the sediment density varies with depth. Since we approximate the sediment body using 100-m-thick 'slivers' of uniform porosity and, hence, density, the technique would require numerous (upwards of 300) separate body computations for each backstrip.

We, therefore, modified the computations so that the sedimentation anomaly can be derived from the rift anomaly, the flexed Moho, and a so-called 'supra-crustal' anomaly.

In the technique of Watts (1988), the present-day anomaly is regarded as the sum of all the geological processes that have modified a margin through time. This is the so-called process-oriented approach to gravity modelling. The sum, in the case of a non-volcanic margin, is then given by:

$$\Delta g_{total} = \Delta g_{rift} + \Delta g_{sedimentation}$$

where Δg_{total} = sum anomaly, Δg_{rift} = rifting anomaly ($\Delta g_{backstrip} + \Delta g_{backstrip\ moho}$), $\Delta g_{sedimentation}$ = sedimentation anomaly, and the backstrip and backstrip moho are as illustrated in Fig. 5. Rearranging gives:

$$\Delta g_{sedimentation} = \Delta g_{total} - \Delta g_{rift}. \quad (3)$$

The sum anomaly at a margin can also be written in an 'object-oriented' form. In this case,

$$\Delta g_{total} = \Delta g_{supra-crustal} + \Delta g_{mantle}$$

where $\Delta g_{supra-crustal} = \Delta g_{topo} + \Delta g_{sediments}$ and $\Delta g_{mantle} = \Delta g_{backstrip\ moho} + \Delta g_{flexed\ moho}$. Or,

$$\Delta g_{total} = \Delta g_{supra-crustal} + \{\Delta g_{backstrip\ moho} + \Delta g_{flexed\ moho}\}, \quad (4)$$

where the flexed Moho is as illustrated in Fig. 5. Substituting (2) in (1) gives:

$$\Delta g_{sedimentation} = \Delta g_{supra-crustal} + \{\Delta g_{backstrip\ moho} + \Delta g_{flexed\ moho} - \Delta g_{rift}\}. \quad (5)$$

Eq. (5) comprises two terms. The first, $\Delta g_{supra-crustal}$, is backstrip independent. The second, between the brackets, depends on the backstrip.

The significance of eqs (4) and (5) is that the sum gravity anomaly can be evaluated without explicit calculation of the sediment body itself for each backstrip. While this does not reduce the total number of bodies, it represents a considerable saving on computational time. This is because the contribution to the sedimentation anomaly of a non-uniform density is only calculated once for a given porosity distribution, rather than for each backstrip.

4.4 Iterative backstripping, gravity modelling, and T_e recovery

In the modelling technique of Watts (1988), the T_e structure is usually estimated by a 'trial-and-error' comparison of observed and calculated gravity anomalies. While this maybe satisfactory on profiles, it is difficult to quantitatively estimate spatial changes in T_e using such an approach.

We, therefore, use an iterative technique to determine the T_e structure *directly* from the observed gravity anomaly. The main difference between our technique and previous ones (e.g. Braitenberg *et al.* 2003) is that the gravity anomaly for different T_e distributions

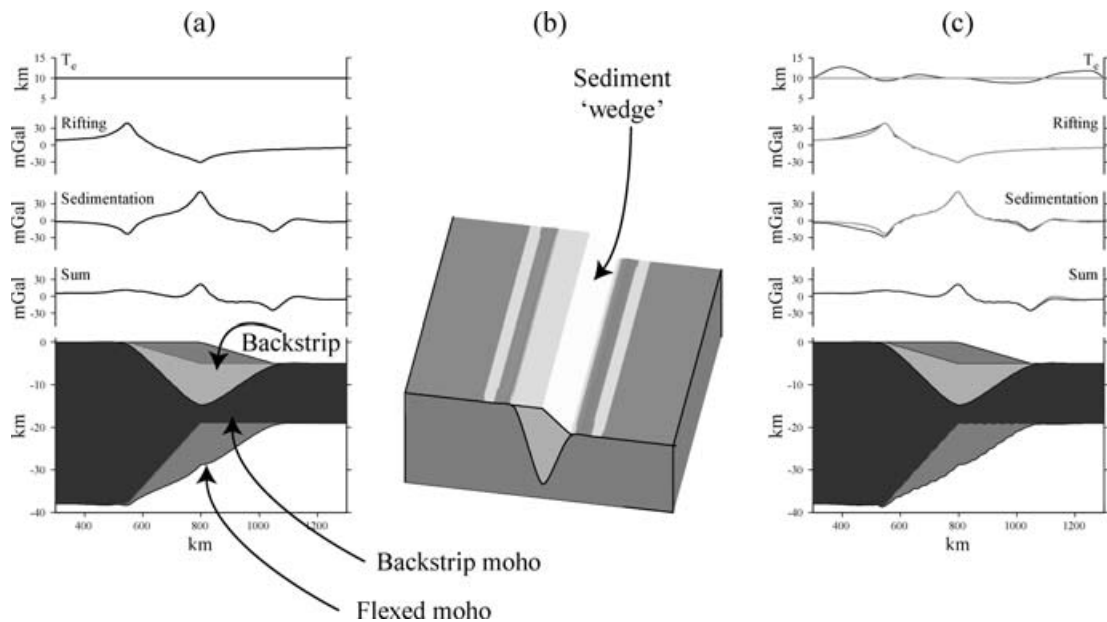


Figure 5. 2-D iterative flexural backstripping and gravity modelling at a synthetic, 270-km-wide, 5-km-deep, margin that formed by crustal thinning at the time of rifting and was then deformed by a 5-km-thick 2-D sediment load. (a) **Forward model** in which the gravity anomalies of the different processes that have modified the margin through time have been calculated using a line-integral method and summed. Rifting anomaly = gravity effect of the thinned crust and its Airy-type compensation. Sedimentation anomaly = gravity effect of the sediment load and its flexural-type compensation ($T_e = 10$ km). Sum anomaly = Rifting anomaly + Sedimentation anomaly. Backstrip = surface obtained by flexurally backstripping the sediments. Backstrip moho = surface obtained by restoring the backstrip using eq. (2). Flexed moho = backstrip moho + flexure due to sediment loading. (b) block model showing geometry of a sediment 'wedge' that has been projected along-strike to form a 3-D margin. (c) **Inverse model** in which T_e distribution is recovered by iteratively backstripping the 3-D sediment grid in b) and comparing the 'observed' sum anomaly (dashed line) to the 'calculated' anomaly (solid line) based on the gravity effect of the backstrip and its Airy-type compensation *and* the gravity effect of the sediment load and its flexural compensation. The figure shows a good general agreement between the recovered T_e and the input T_e . Uniform densities of 1030, 2600, 2850 and 3330 kg m⁻³ have been assumed for the water, sediment, crust and mantle, respectively.

is repeatedly computed and compared to the observed. The best-fit T_e structure is then estimated and used as an input for the next iteration.

The details of the iterative technique are described in Wyer (2003) and so will only be briefly outlined here. The first step is to determine the uniform T_e in steps of 1 km between 0 and 100 km that best minimizes the rms difference between observed and calculated free-air gravity anomalies within individual sliding, overlapping, windows. We tested a range of different window sizes, but found that a 0.5° (longitude) × 0.2° (latitude) window yielded the most rapid convergence. T_e estimates centred in their respective windows are then gridded (using GMT surface) with a small tension ($T = 0.1$) in order to retain minimum and maximum values. The second step is to filter the T_e grid using a bandpass filter (cut wavelengths <100 km, pass wavelengths >500 km with cosine taper in between) in order to avoid instabilities in the derivative calculations due to abrupt changes and then to use a spatially variable T_e model to calculate the flexure and, hence, gravity anomaly. Finally, the T_e distribution is perturbed by ± 5 km ($T_e \geq 0$ km) in 1 km intervals to give a suite of 11 windowed rms difference anomalies with which to refine the T_e distribution for the next iteration.

We tested the combined backstripping and iterative gravity modelling technique at a uniform T_e , synthetic margin loaded by a 2-D sediment wedge, of similar cross-sectional profile to that at the East Coast, USA margin. As Fig. 5 shows, the technique successfully recovers the input T_e structure, except in the region flanking the sediment load where there are small deviations from the input T_e .

The test in Fig. 5 is limited in that it does not illustrate the ability of the technique to recover a spatially varying T_e structure. We, therefore, placed the 2-D sediment wedge load on the surface of an elastic plate with a T_e structure that varied both across-strike and along-strike a margin and calculated the rifting, sedimentation and sum gravity anomalies. The sum gravity anomaly grid was then used, together with the accompanying sediment thickness grid, to recover the T_e structure.

Fig. 6 shows that, even with 10 per cent random noise applied to the sum gravity anomaly and the sediment grids, the iterative technique recovers well an input spatially varying T_e structure, except over the regions flanking the load. In particular, the technique recovers well both the amplitude and wavelength of the input T_e . The main departures are at the boundaries of low and high T_e , where the inverted T_e changes more slowly than the input T_e . The rms difference between input and recovered T_e within the bounds of the load, however, is smaller than 5 km.

That the iterative comparison of observed and calculated gravity anomalies is able to recover a spatially varying T_e structure has recently been illustrated in a study by Jordan & Watts (2005) of peninsula India and Tibet. These authors showed good agreement between the results of 2-D forward modelling and a slightly modified version of the 3-D inverse, iterative, technique described in Wyer (2003) and used in this paper, recovering a T_e structure that varied from a few km to >100 km over horizontal spatial scales as small as 100 km.

We recognize, of course, that such applications of the iterative technique assume that surface loads are compensated by flexure

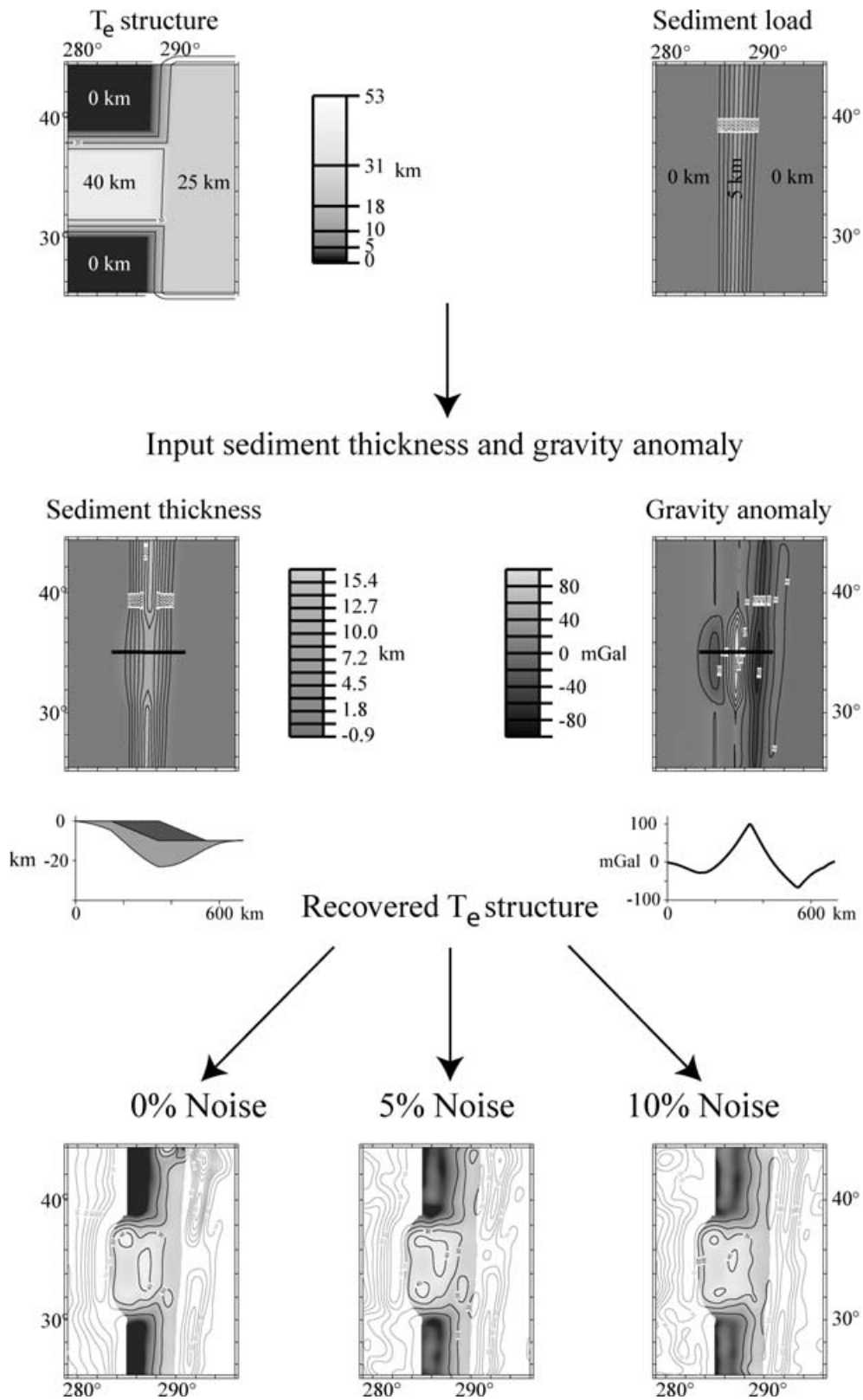


Figure 6. 3-D iterative flexural backstripping and gravity modelling at a synthetic, 270-km-wide, 5-km-deep, margin in which a 5-km-thick 2-D sediment ‘wedge’ loaded a basement with a spatially varying T_e . Top 2 panels show the T_e structure, which varies across-strike and along-strike the margin, and the sediment load. Middle panels show the associated sediment thickness (obtained by adding the sediment load to the flexure) and the sum gravity anomaly (i.e. the sum of the rifting and sedimentation anomaly). The solid lines show the location of the profiles. Bottom panels show the T_e recovered using the sediment thickness and sum gravity anomaly data for different levels of noise in the sediment thickness and gravity anomaly data.

and that there is little or no contribution to the gravity anomaly from lateral density contrasts or other factors. Nevertheless, we believe that the technique is a useful new way to determine the T_e structure necessary to explain gravity anomaly data and to derive the long-term thermal and mechanical properties of rifted lithosphere.

5 APPLICATION TO PROFILES

Fig. 7 shows the results of applying the 3-D combined backstripping and iterative gravity modelling technique to 4 profiles of the East Coast, USA margin. These profiles have been chosen because seismic reflection and refraction data have already been acquired

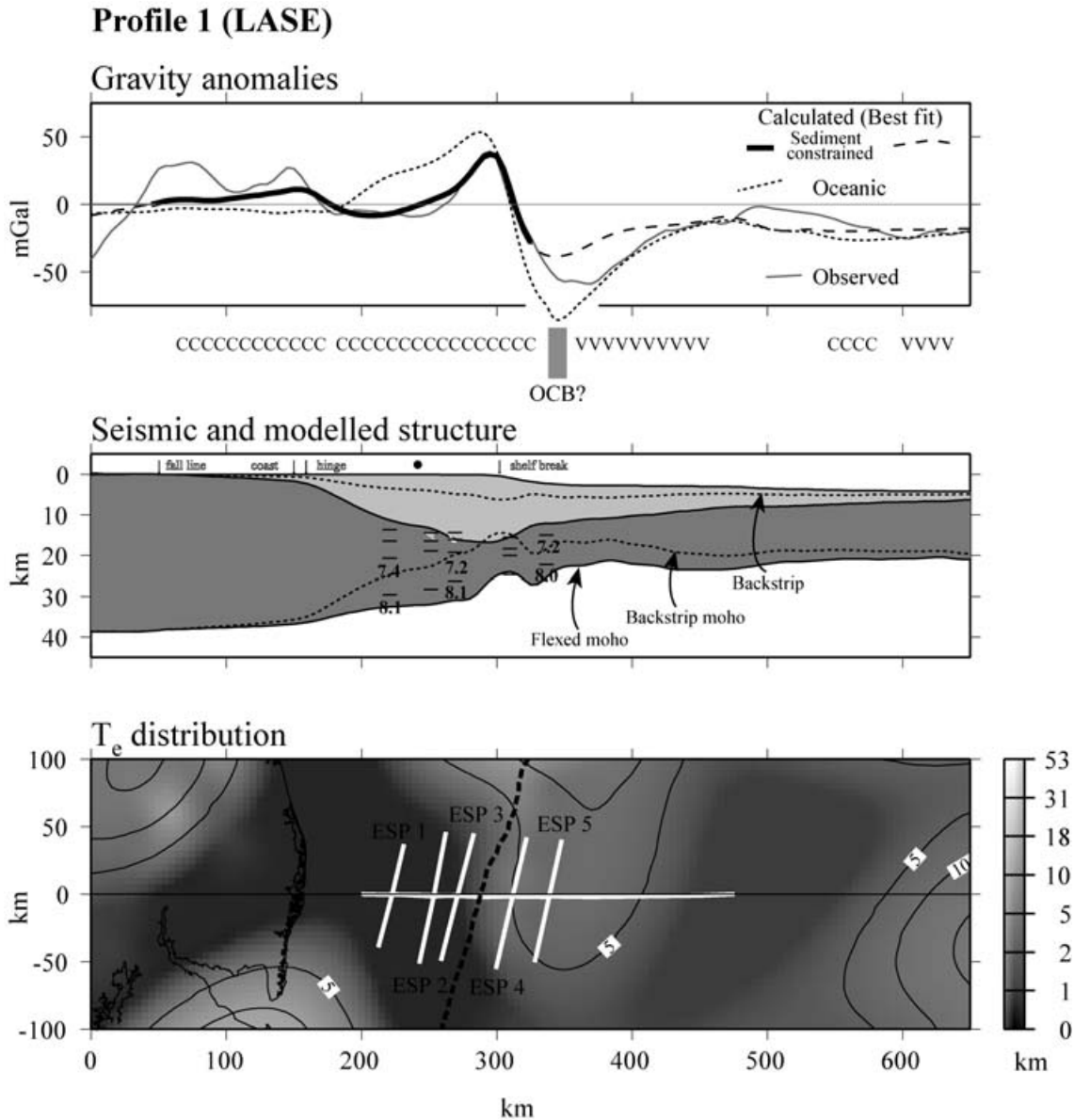


Figure 7. The application of the 3-D iterative flexural backstripping and gravity modelling technique to Profiles 1–4 (Fig. 1c). (a) Profile 1 which follows the LASE seismic refraction profile (LASE study group 1986). The upper profile compares observed and calculated free-air gravity anomalies. The observed anomaly (thin solid line) is based on the gravity anomaly grid in Fig. 1. The calculated anomalies (thick solid line = region between the Fall line and easternmost edge of the USGS multichannel seismic reflection surveys where there is good sediment thickness control, wide dashed line = peripheral regions) are based on the ‘best-fit’ T_e distribution and an oceanic case in which $T_e = Z_{450}$ (narrow dashed line). C = Region of the profile where the ‘best-fit’ explains the observed data better than the oceanic case. V = Region of the profile where the oceanic case explains the observed data better than the ‘best-fit’ case. The middle profile shows the predicted crustal structure based on the ‘best-fit’ T_e distribution compared with seismic refraction data. Upper dashed line = sediment backstrip. Lower dashed line = backstrip Moho. Horizontal bars indicate major velocity gradients. Selected P -wave velocities (km s^{-1}) are shown in bold. Filled circle = East Coast Magnetic Anomaly (ECMA). The lower profile shows the ‘best-fit’ T_e distribution along and up to 100 km either side of the profile. (b) Profile 2 which follows the EDGE-801 seismic refraction profile (Holbrook *et al.* 1994a). Dipping white lines (middle profile) = seaward-dipping reflectors (SDRs). Symbols as in (a). (c) Profile 3 which follows the USGS32 seismic refraction profile (Trehu *et al.* 1989). Symbols as in (a). Dipping white lines and shading as in (b). Filled square = Brunswick Magnetic Anomaly. Filled star = Blake Spur Magnetic Anomaly. (d) Profile 4 which follows the BA-6 seismic refraction profile (Holbrook *et al.* 1994b). Symbols as in (a) and (c). Dipping white lines and shading as in (b).

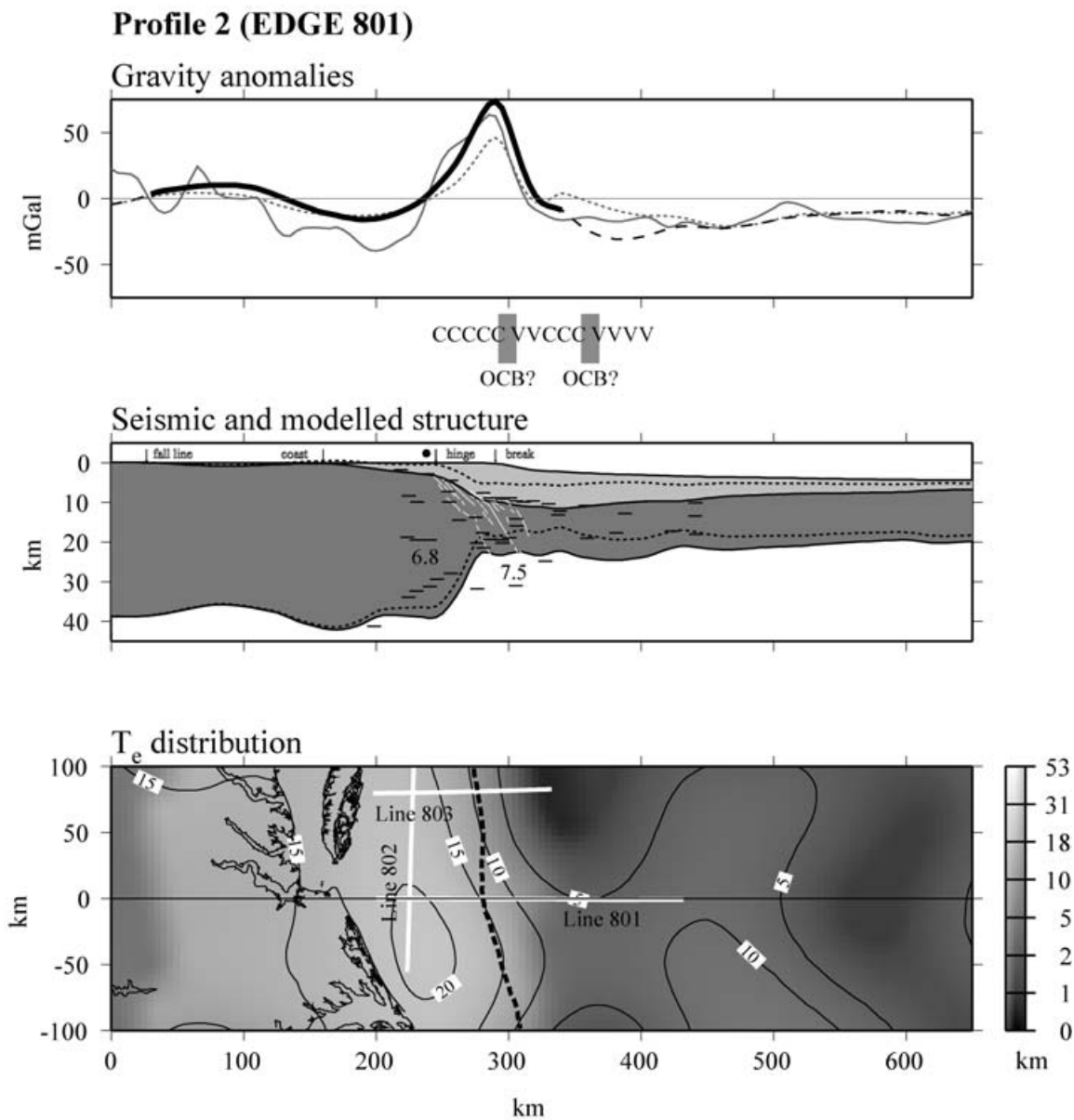


Figure 7. (Continued.)

along them. The figure compares the calculated and observed gravity anomaly and crustal structure along each profile and shows the 'best-fit' T_e structure within a 100 km window either side of the profile.

5.1 Profile 1—LASE-6

Profile 1 (Fig. 1c) crosses the northern part of the USA margin in the region of the Baltimore Canyon Trough where it follows the LASE-6 (LASE study group 1986) coincident seismic reflection and refraction profile. These data indicate a sediment thickness of up to 15 km that is underlain by relatively thin (8–10 km), high velocity (P wave velocity of 7.0–7.5 km s⁻¹) crust.

Fig. 7(a) shows good agreement between the observed and calculated free-air gravity anomalies based on the 'best-fit' T_e structure. In particular, the calculated anomaly explains well the amplitude and wavelength of the edge effect high and the low that flanks its

landward side. The main discrepancies are west of the coastline, between 0 and 175 km along the profile, where the observed anomaly is significantly higher than the calculated, and east of the shelf break, between 320 km and 450 km, where the observed anomaly is significantly lower. We attribute the high west of the coastline to a mass excess in the basement that underlies the coastal plain at relatively shallow depths.

The low in the region of the continental rise could also result from lateral density changes in the underlying basement. Another possibility, is that it is due to flexural loading of a basement that increases its T_e with time. We have, therefore, computed the gravity anomaly (narrow dashed line, Fig. 7a) that would be expected if the sediments loaded oceanic basement that increases its T_e as it cools away from a mid-ocean ridge (Watts 1978). Fig. 7(a) shows an excellent agreement between the observed and calculated gravity anomalies in the region of the low that flanks the edge high on its seaward side, suggesting that oceanic basement underlies sediments

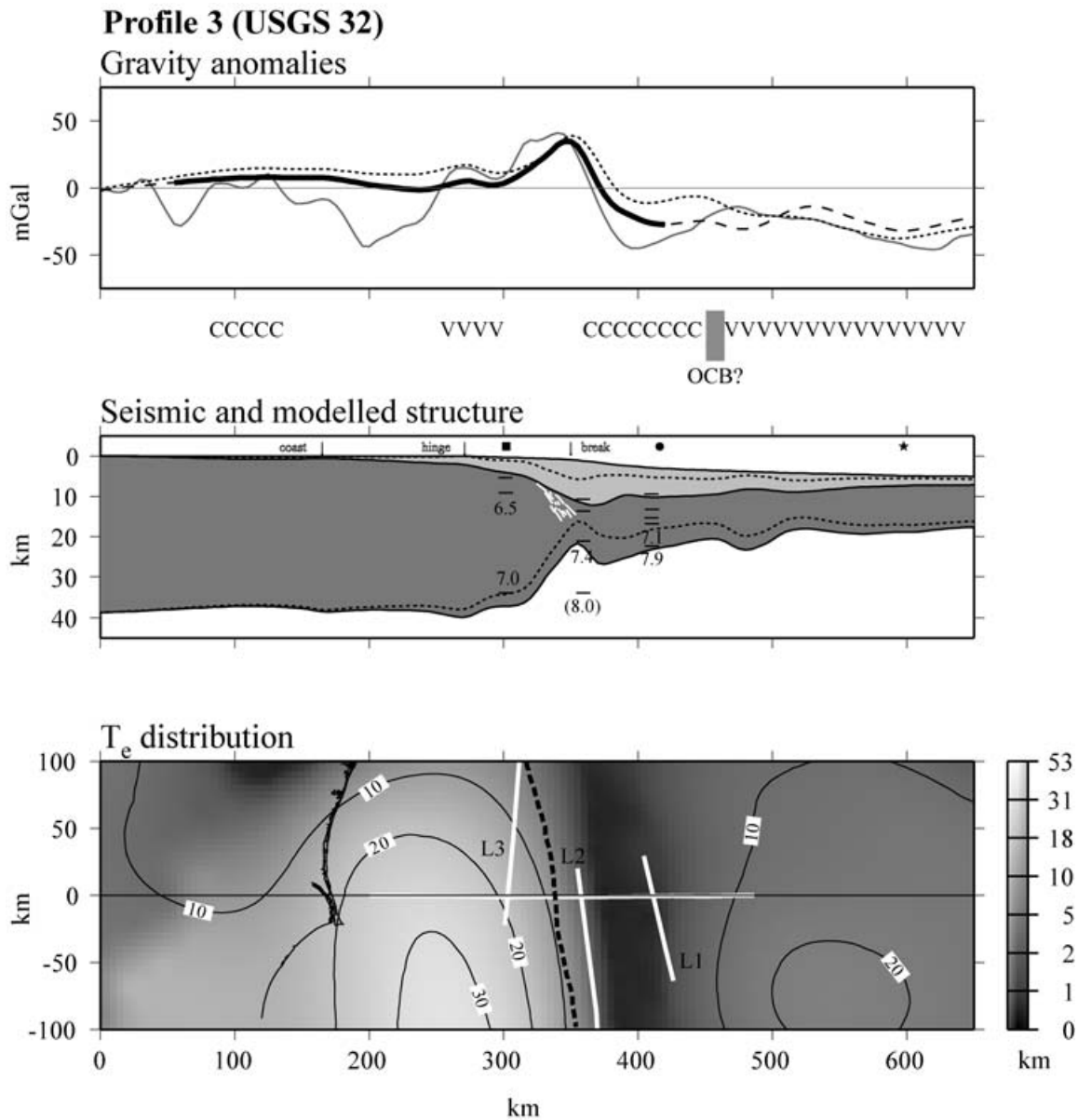


Figure 7. (Continued.)

beneath the rise region. The figure also shows that a T_e that increases with time is unable to account for the low that flanks the edge high on its landward side.

The 'best-fit' T_e structure in the region of Profile 1 suggests low average values ($0 < T_e < 10$ km) over the shelf, slope and upper rise. The low values correlate with a region of relatively thin crust that we interpret as partly highly attenuated continental crust and partly oceanic crust. If T_e of both attenuated lithosphere and oceanic lithosphere is small initially and then increases with age as it cools with time then, the low values could be caused by a higher sediment accumulation during the early history of the margin than during its later history.

The crustal structure implied by the 'best-fit' T_e structure agrees reasonably well with the seismic structure. The seaward thinning of the crust is explained. The main departures are in the Moho depth and the flexed Moho is deeper (by up to 5 km) than the seismic Moho.

5.2 Profile 2—EDGE 801

Profile 2 (Fig. 1c) crosses the central part of the East Coast USA margin offshore Virginia where it follows the EDGE 801 seismic reflection and refraction profile (Sheridan *et al.* 1993; Holbrook *et al.* 1994a). These data indicate a post-rift sediment thickness of up to 8 km that is underlain by a highly reflective 6.3–6.7 km s⁻¹ mid-crustal layer. The lower crust is associated with velocities in the range 6.8–7.5 km s⁻¹, with the highest velocities occurring beneath the slope and rise.

Fig. 7(b) shows good agreement between the observed and calculated free-air gravity anomalies based on the best-fit T_e structure in the region. The calculated anomaly explains the amplitude and wavelength of the edge high, although its landward gradient differs from that of the observed. The main discrepancies are east of the hinge zone, between 225 km and 260 km, where the observed anomaly is slightly higher than is calculated and west of the hinge

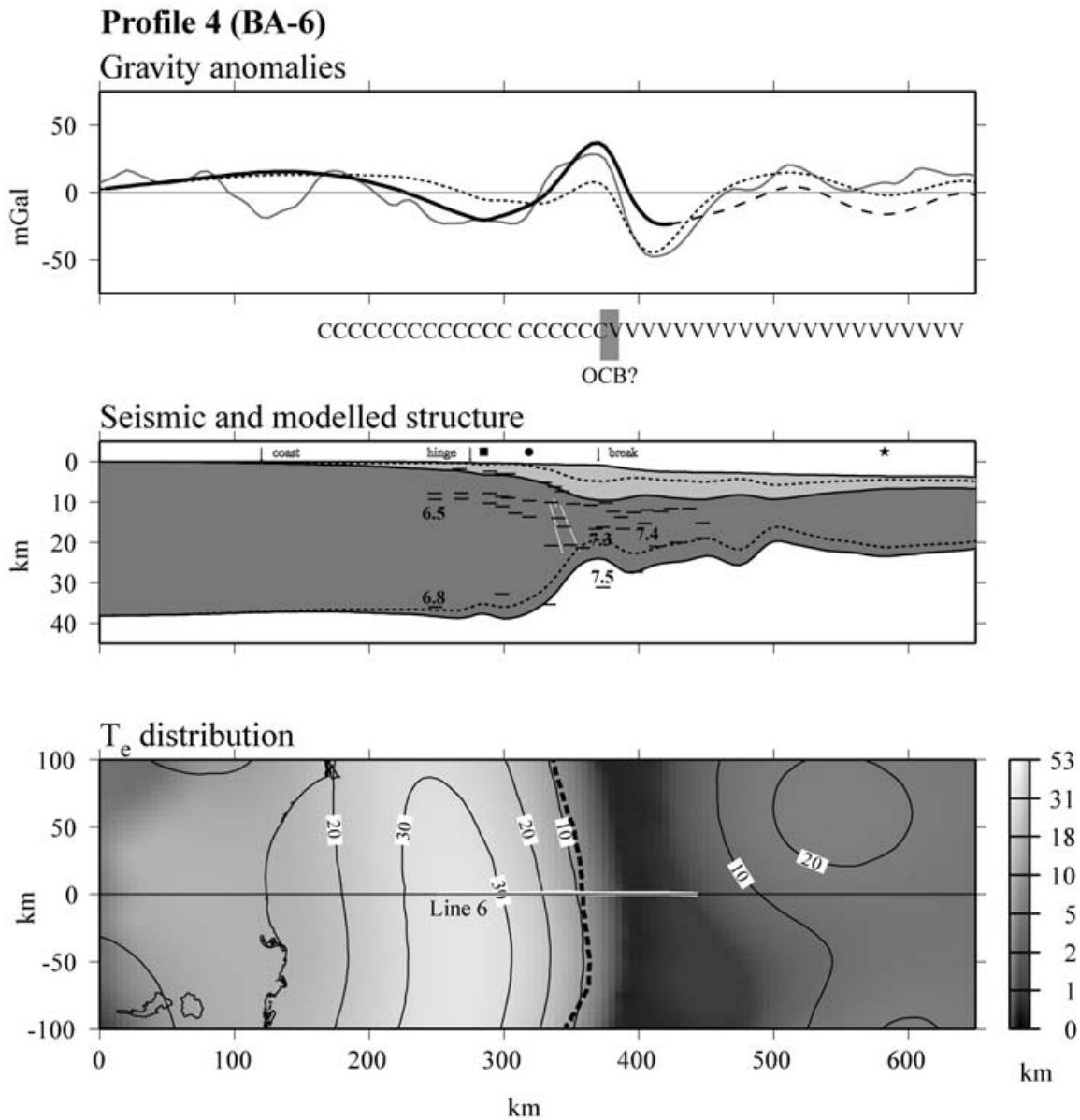


Figure 7. (Continued.)

zone, between 110 km and 250 km where the anomaly is significantly less. We attribute the high and low to lateral density changes in the underlying basement.

There is no evidence that a T_e that increases with time improves the fit between observed and calculated gravity anomalies along any part of the profile. Indeed, there is a suggestion that a T_e that increases with time actually makes the fit worse in the region of the edge high.

The ‘best-fit’ T_e structure along Profile 2 suggests high average T_e values over the shelf and upper slope ($T_e > 15$ km) and low values ($T_e < 5$ km) over the rise. The high values correlate with thick crust beneath the Carolina platform and we attribute them to relatively unstretched continental crust. The low values correlate with thin crust and, as in Profile 1, we attribute them to a significant component of sediment loading on either attenuated crust or relatively young oceanic crust.

The crustal model, unlike for Profile 1, fits the seismic structure poorly. The main departures are between 210 km and 265 km and

325 km and 440 km where the flexed Moho is deeper than the seismic Moho. The most significant departure, however, is between 260 km and 340 km where the seismic Moho is up to 12 km deeper than the flexed Moho.

5.3 Profile 3—USGS32

Profile 3 (Fig. 1c) crosses the southern part of the East Coast, USA margin offshore Carolina in the region of the Carolina platform and trough where it follows USGS 32 seismic reflection profile (Klitgord *et al.* 1988). Intersecting the profile are 3 large-offset refraction profiles (Trehu *et al.* 1989). These data indicate a post-rift sediment thickness of up to 13 km that is underlain by a 6.1–7.1 km s⁻¹ crust and a lower crustal ‘lens’ with velocities >7.2 km s⁻¹, which extends from beneath the Carolina trough to the adjacent oceanic crust.

Fig. 7(c) shows general agreement between the observed and calculated free-air gravity anomalies based on the ‘best-fit’ T_e structure. The calculated anomaly explains the amplitude of the edge high,

although both its landward and seaward gradients differ from the observed. The main discrepancies are again to the east of the hinge zone, between 260 and 350 km, where the observed anomaly is higher than the calculated and west of the hinge zone, between 50 and 250 km, where the observed anomaly is significantly less. The pattern of anomalies landward of the edge high is, therefore, similar to Profile 2.

There is no evidence that a T_e that increases with time improves the fit between observed and calculated gravity anomalies, except for a short segment of the profile in the region of the middle rise. There is again the suggestion that a T_e that increases with time actually makes the fit worse over the region landward of the edge high and over the slope and upper rise.

The 'best-fit' T_e structure along Profile 3 is similar to Profile 2. The high values again correlate with relatively thick crust that underlies the Carolina platform and we attribute them to relatively unstretched continental crust. The low values correlate with thin crust and we again attribute them to a significant component of sediment loading on relatively young oceanic crust.

The crustal model fits the seismic structure reasonably well (to better than 5 km) beneath the shelf at 300 km, and upper rise, at 405 km. There is a large departure, however, beneath the upper part of the slope, at 350 km, where the seismic Moho is deeper than the flexed Moho by >12 km.

5.4 Profile 4—BA-6

Profile 4 (Fig. 1c) crosses the southern part of the East Coast, USA margin offshore Carolina in the region of the Carolina platform and trough where it follows the co-incident BA-6 seismic reflection and refraction profile (Holbrook *et al.* 1994b). These data indicate a post-rift sediment thickness of up to 12 km that is underlain by mid-crustal reflections, a 6.5–6.9 km s⁻¹ crust and a lower crustal body with velocities 7.2–7.5 km s⁻¹.

Fig. 7(d) shows overall agreement between the observed and calculated free-air gravity anomalies based on the best-fit T_e structure. The calculated anomaly explains the amplitude of the edge high, but its seaward gradient is less steep and appears, as in Profiles 2 and 3, to be shifted seaward of the observed. Unlike Profiles 2 and 3, however, the landward low is now fit reasonably well. The main discrepancies are seaward of the shelf-break, between 380 and 440 km, where the observed anomaly is significantly less than the calculated.

A T_e that increases with time significantly improves the fit between observed and calculated gravity anomalies seaward of the upper slope. Moreover, a T_e that increases with time actually makes the fit worse in the region of the edge high and the landward flanking low.

The 'best-fit' T_e structure along Profile 4 is similar to Profiles 2 and 3 and suggests high average T_e values over the shelf and low values over the rise.

The crustal model again fits the seismic structure reasonably well beneath the shelf and upper rise. There is a large departure, however, beneath the upper part of the slope, at 375 km, where the seismic Moho is deeper than the flexed Moho by ~8 km.

6 SENSITIVITY

The calculated free-air gravity anomaly profiles in Fig. 7 are based on a 'standard' model with an assumed density of 2720, 2850, 3300 kg m⁻³ for sediment (grains), crust and mantle, respectively, an Athy-type porosity versus depth distribution (with $\phi_0 = 0.15$ and

$Z = 4629$ m for the surface porosity and compaction depth constant, respectively), a zero-elevation crustal thickness of 38 km, and a T_e structure that varies both spatially and temporally.

Fig. 8 shows the sensitivity of the rms difference between observed and calculated gravity anomalies to changes in these model parameters. The figure suggests that the strongest sensitivity is to changes in T_e . There is also quite a strong sensitivity to the porosity parameters with $\phi_0 > 0.25$ and $Z < 1000$ m giving high rms. Otherwise, the weakest sensitivity is to the sediment (grains), crustal and mantle density and the zero-elevation crustal thickness.

7 T_e STRUCTURE OF THE MARGIN

Fig. 9 shows the best-fit T_e structure determined from backstripping and gravity modelling along the East Coast, USA margin. We only show the T_e structure for the region of the margin where there is adequate control on the sediment thickness from seismic reflection profile, well or other sample data. This includes the region of the coastal plain, the shelf and a portion of the slope and rise.

The figure shows a large variation in T_e both across-strike and along-strike the margin. T_e appears to correlate with the embayment and arch structures inferred by Brown *et al.* (1972) from stratigraphic studies of the coastal plain. Low T_e (<10 km) correlates with the Alberbarle and Raritan embayments. High T_e (>10 km) correlates with the Cape Fear Arch, Norfolk High and Long Island Platform. The main exception is the Salisbury embayment that is a region of intermediate T_e .

There is little correlation, in contrast, between T_e and the present-day morphology of the margin. The shelf break, for example, correlates with a wide range of T_e values. The best correlation appears with the structural elements of the margin. The $T_e = 10$ km contour, for example, generally follows the arch and embayment structure along the margin.

Fig. 9 shows that spatial variations in T_e extend beyond the shelf break, across the slope to the upper part of the continental rise. We note from Fig. 7, however, that in rise regions a model with a T_e that is dependant on age since rifting generally fits the observed gravity anomaly data better than one that is based on a single, average, T_e value. We attribute this to the fact that oceanic crust probably underlies much of the continental rise. It is interesting that the 'best-fit' single T_e value in the rise region is so low (<5 km). This suggests to us that not only are such values temporal averages, but that they may be biased downwards and mainly reflect the response of the margin to voluminous sediment loading early in its history.

The reliability of the T_e structure in Fig. 9 can be assessed by consideration of its stability and sensitivity. The stability, which we define as the change in the T_e structure over successive iterations, and the sensitivity, which we define as the change in the rms deviation in the flexural isostatic gravity anomaly to small shifts in the T_e structure, are shown in the insets in Fig. 9. The insets show that both the T_e structure and the rms deviation decrease with increase in the number of iterations. The change in T_e structure decreases most rapidly, after which the rms deviation continues to decrease as the iterative scheme resolves a finer T_e structure. After ~10 iterations the change in T_e structure is negligible and the final rms deviation is 18.7 MGal, which is significantly less than for the Airy case (29.3 MGal).

Finally, we have tested the dependence of the 'best-fit' T_e structure on the initial input T_e distribution. Initiating the iterative process with a range of high and low uniform T_e distributions reproduces

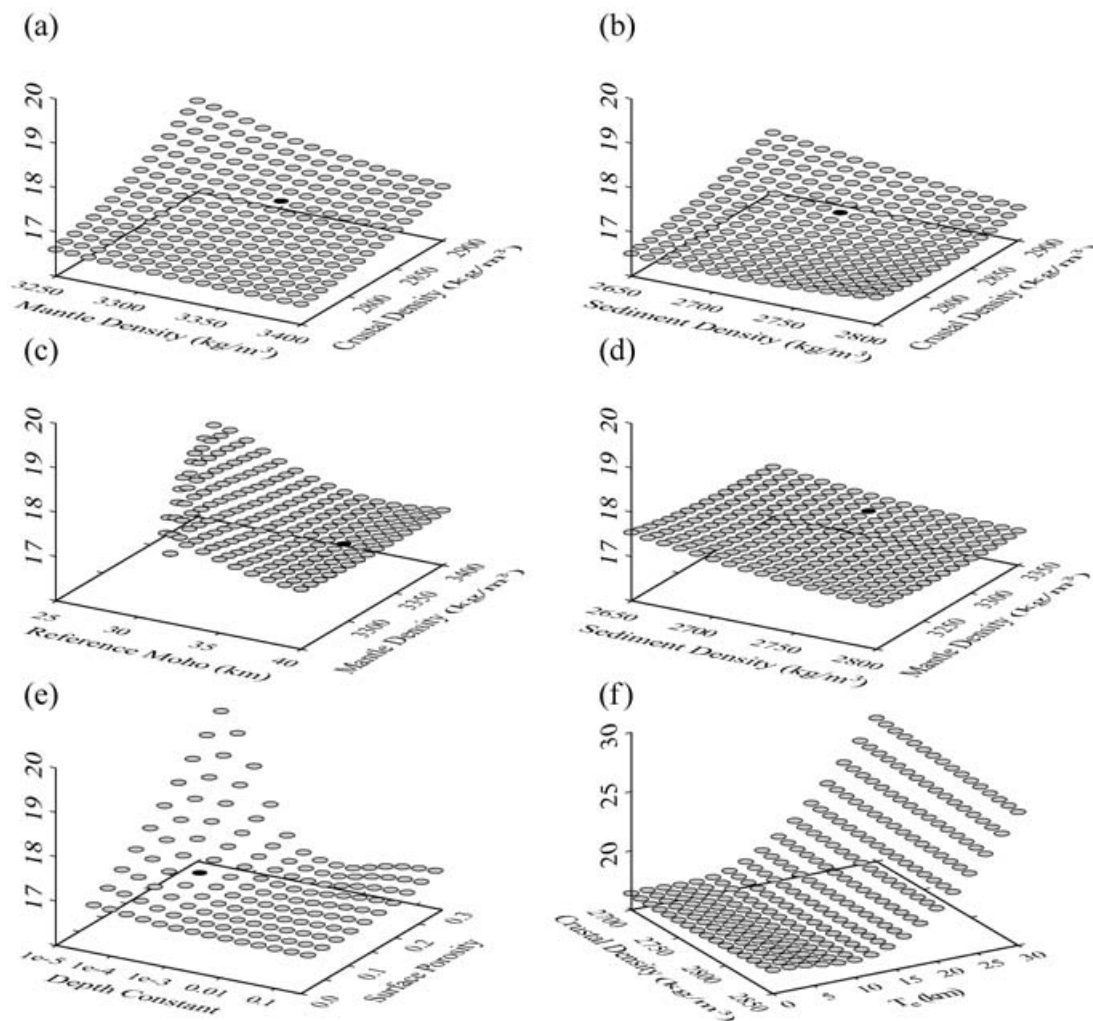


Figure 8. Plot showing the rms difference between observed and calculated free-air gravity anomalies in MGal (z -axis) as a function of the main model parameters (x - and y -axis). The rms has been computed for a limited region where there is reliable sediment thickness data (e.g. Fig. 9). Filled ellipses in the plots in (a)–(e) show the ‘standard’ values used in Fig. 7 to derive the T_e structure. We assumed $T_e = 0$ in the plots in (a)–(e). (a) mantle and crustal density. (b) sediment and crustal density. (c) zero elevation crustal thickness and mantle density. (d) sediment and mantle density. (e) sediment porosity depth constant and sediment surface porosity. (f) crustal density and T_e . The z -axis scale is the same in plots (a) to (e), but has been reduced in (f) because of the strong dependence of the rms on T_e .

the final gross T_e structure presented here, but greatly increases the number of iterations required for convergence.

8 DISCUSSION

8.1 Comparison to previous studies

There have been only a few previous estimates of the T_e structure of the East Coast, USA margin and none have been carried out in 3-D. The results of this study are, however, in broad agreement with the existing 2-D results of Watts (1988) for the Baltimore Canyon Trough and Pazzaglia & Gardner (1994) for the Salisbury embayment— T_e is relatively low over the Baltimore Canyon Trough and high over the Salisbury embayment. We agree with the magnitude of the low over the Baltimore Canyon Trough (<5 km), but disagree with the magnitude of the high over the Salisbury embayment (10–20 km—this paper, ~40 km—Pazzaglia & Gardner (1994)). This difference is attributed to the fact that our T_e structure reflects the average response of the margin to sediment load-

ing since the Late Triassic/Early Jurassic whereas the Pazzaglia & Gardner (1994) value reflects sediment loading and erosional unloading since the Late Cenozoic.

8.2 Relationship of T_e to stretching and curvature

Dynamical models for the initiation of rifting suggest there should be certain links between the strength of the lithosphere and the amounts of extension (e.g. Burov & Poliakov 2001). For example, some correlation might be expected between T_e and β , especially since T_e maybe an inherited feature that is a proxy for the strength of the pre-rift lithosphere. Inherited T_e may control, for example, the distribution of extension: low T_e lithosphere is weaker and would be expected to extend over a wide region whilst high T_e lithosphere is stronger and would be expected to extend over a narrower, more focused, region.

Fig. 10 shows that there is a general decrease in T_e with increase in β at the East Coast, USA margin. The ‘threshold’ T_e is given approximately by $50/\beta$. The data below this threshold, however,

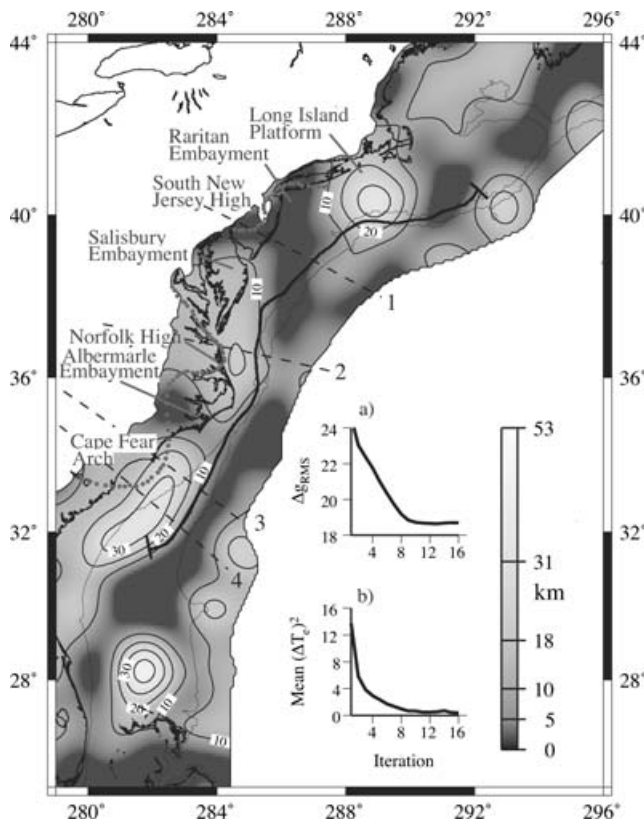


Figure 9. The recovered T_e distribution in those regions of the margin where there is reliable sediment thickness data. The structural highs and lows (i.e. promontories and embayments) are based on Figure 2-1 of Owens & Gohn (1985). The insets show details of the T_e recovery. The solid black line locates the profile in Fig. 13. The dashed black lines locate Profiles 1–4 in Fig. 7. (a) Plot of rms of the flexural isostatic anomaly versus number of iterations. The rms has been computed for the entire grid area (e.g. Fig. 1). The rms for $T_e = 0$ km (i.e. Airy model) = 29.3 MGal. Note that for iterations > 8 there is little subsequent reduction in the flexural isostatic anomaly. (b) Plot of the change in recovered T_e versus number of iterations. Note that for iterations > 8 there is little subsequent change in the T_e distribution.

shows considerable scatter, presumably because the inherited integrated strength is variable across-strike and along-strike the margin.

We might also expect some correlation between T_e and the amount of sediment loading. This is because sediment loading would increase the deformation and, hence, curvature, K , of a flexed plate which Yield Strength Envelope (YSE) considerations (e.g. Goetze & Evans 1979) suggest might yield, thereby reducing T_e (e.g. Burov & Diament 1995). This effect is seen in observed data. For example, the Apennine and Dinaride foreland basins have high K and low T_e (Kruse & Royden 1994) while the sub-Andean basins have low K and high T_e (Stewart & Watts 1997).

Fig. 11 shows that there is a general decrease in T_e with increase in K . There is a ‘threshold’ T_e that is similar to what would be expected for a YSE model. The data below the threshold again show considerable scatter, but the effect of curvature becomes increasingly dominant beyond $\sim 10^{-6} \text{ m}^{-1}$.

It is interesting to note from Fig. 11 that plate curvatures at the East Coast, USA margin range up to values $\sim 10^{-5} \text{ m}^{-1}$. These are among the largest values that have been reported from flexural loading, exceeding those at deep-sea trench outer rises (e.g. McNutt & Menard 1982) and foreland basins (e.g. Kruse & Royden 1994). It is clear from YSE considerations (e.g. Watts & Burov 2003) that cur-

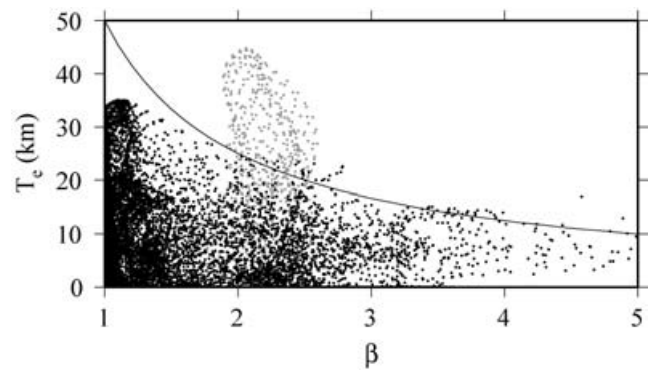


Figure 10. Plot of T_e against β , the amount of stretching, along the East Coast, USA margin. The T_e is based on Fig. 9. The β has been calculated from the zero-elevation crustal thickness and the vertical distance between the sediment backstrip and the backstrip Moho. The solid line shows a calculated curve in which T_e is given by $50/\beta$. Most of the data are enveloped by the curve. The main exceptions are data from the Blake Plateau (light grey dots). However, the sediment thickness is not well constrained in this region.

vatures this high would result in very low T_e and, hence, integrated strength of the lithosphere. Indeed, some workers (e.g. Erickson 1993) have already speculated that weakening of the lithosphere by sediment loads at rifted margins may be one of the principal factors that could initiate subduction and lead to the closure of an ocean basin.

8.3 Other controls on T_e

It is clear from the scatter in Figs 10 and 11 that curvature and stretching are not the only factors that control the T_e at rifted margins. The YSE model predictions in Fig. 11, for example, are based on an assumed crustal and upper mantle composition, geothermal gradient, strain rate and, hence, rheological structure. They also assume that post-rift processes such as sedimentation and erosion do not ‘feed back’ to alter the basic rheological structure.

The East Coast, USA margin is highly segmented along-strike, as seen in its promontory and embayment structure (e.g. Brown *et al.* 1972). These features could be associated with pre-existing changes in either the compositional or the thermal and mechanical structure of the underlying basement. For example, Noltimier *et al.* (2004) have noted that there are NW-SE trending topographic features in the Precambrian basement associated with the East Continent Rift Valley in Ohio and Thomas (2006), among others, have pointed out the significance of NW-SE trending transform faults in the early opening of the proto-Atlantic ocean and the development of the Iapetan rifted margin. Such features could, we speculate, have influenced the long-term strength, as well as the mode of extension, of the East Coast, USA rifted margin.

8.4 Isostatic gravity anomalies

The role of flexure at the East Coast, USA margin can, perhaps, be best assessed from a consideration of the isostatic gravity anomaly. We consider first the ‘classical’ Airy isostatic anomaly, defined as the difference between the observed free-gravity anomaly and the gravity effect of the topography and its Airy-type compensation.

Behn & Lin (2000) showed that a ‘classical’ Airy model, which includes a correction for the sediment thickness, significantly reduces the magnitude of the free-air anomaly edge effect ‘couple’ at the margin. However, as Fig. 12b shows the ‘couple’ is still visible in

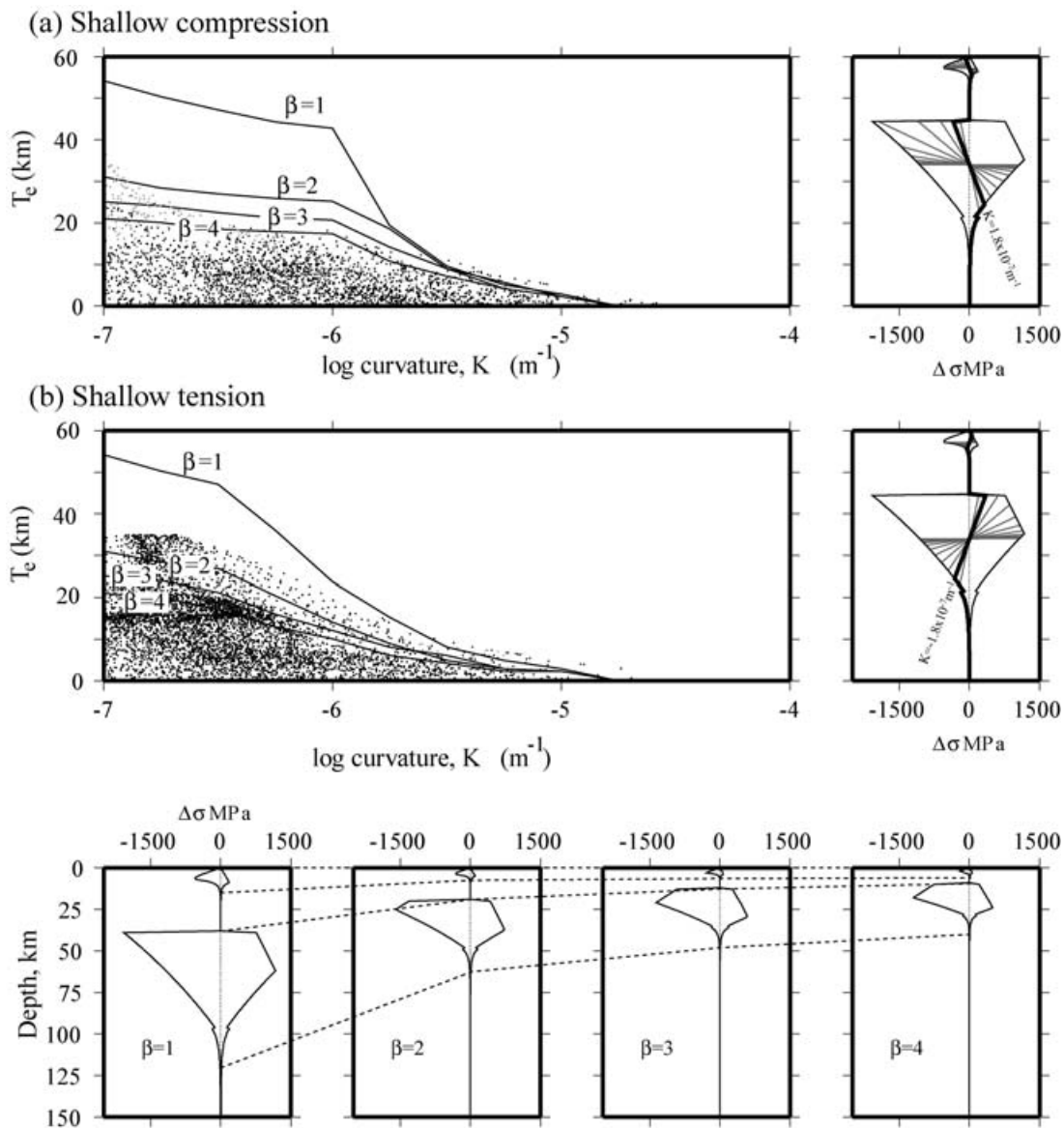


Figure 11. Plot of T_e against $\log |K|$, the curvature of the flexed basement, along the East Coast, USA margin. (a) Positive curvatures (i.e. $K > 0$) which yield strength envelope (YSE) considerations suggest correspond to shallow compression. (b) Negative curvatures which YSE considerations suggest correspond to shallow tension. Insets show the YSE for $\beta = 1$, a crustal thickness of 35 km, a quartz upper crust, a diabase lower crust, a olivine mantle and a strain rate of $1 \times 10^{-15} s^{-1}$. Solid lines show the expected relationship between T_e against $\log K$ for $\beta = 1, 2, 3$ and 4.

the Airy isostatic anomaly. Moreover, several large-amplitude (± 30 MGal) positive and negative isostatic anomalies remain, the most prominent of which correlate with the Long Island Platform, the Norfolk High, and the Cape Fear Arch.

In order to determine the origin of these anomalies, we compare in Fig. 12 the free-air anomaly to an isostatic anomaly based on our recovered T_e structure. The anomaly, which we dub the flexural isostatic anomaly, is defined as the difference between the observed free-gravity anomaly and the gravity effect of the topography and sediment and their flexural-type compensation. The figure shows that the flexural isostatic anomaly is generally of smaller amplitude than the Airy isostatic anomaly and that the free-air anomaly edge effect ‘couple’ offshore Delaware, New Jersey and New York is nearly completely removed in the flexural isostatic anomaly.

Fig. 13 compares the flexural and the Airy isostatic anomalies along a profile that follows the peak of the isostatic edge ef-

fect anomaly ‘high’. Figs 13(a) and (b) (solid lines) shows the Airy isostatic anomaly based on Behn & Lin (2000) and this paper, respectively. The two profiles agree closely and show that the margin correlates with large-amplitude (± 25 mGal) Airy isostatic anomalies. The incorporation of an Athy-type Porosity versus depth function (dashed line in Fig. 13b) reduces the amplitude of the Airy isostatic anomaly somewhat over the deepest part of the basins, but large-amplitude anomalies remain. Fig. 13c shows that the flexural isostatic anomaly based on the T_e structure in Fig. 9 is significantly more subdued than the Airy isostatic anomaly, suggesting that the flexure model is a better description of the state of isostasy at the East Coast, USA margin than the Airy model.

The role of flexure is particularly well seen in power spectra plots. Figs 13(a)–(c) compares power spectra plots for the Airy and flexural isostatic anomalies. Both Airy isostatic anomaly profiles

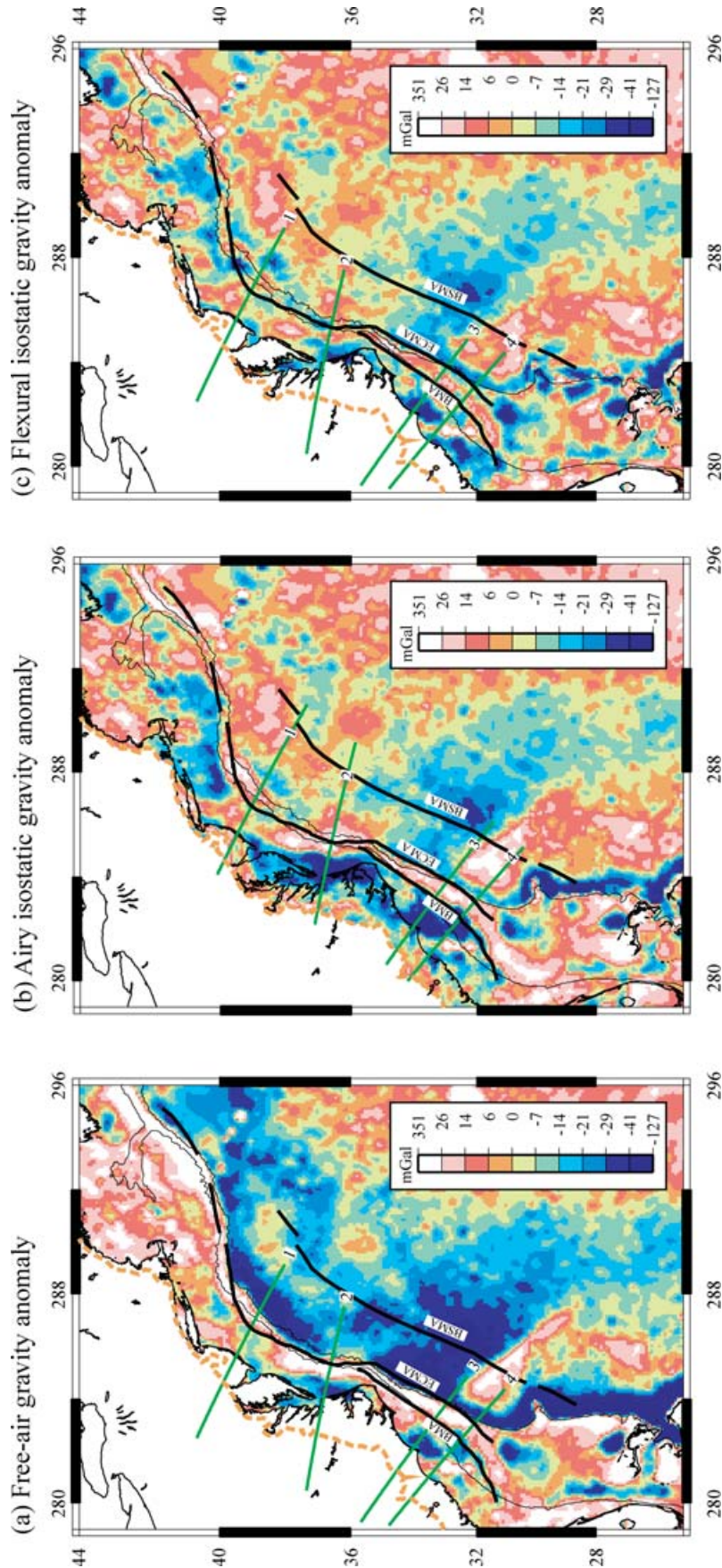


Figure 12. Comparison of the free-air, Airy isostatic and ‘best-fit’ flexural isostatic gravity anomalies. The free-air anomaly is based on the DNAG data set with the degree and order 16 field of Rapp & Pavlis (1990) removed. The Airy isostatic anomaly is based on an assumed density of 2720, 2850, 3300 kg m⁻³ for sediment (grains), crust and mantle, respectively, an Athy-type porosity versus depth distribution (with $\phi_0 = 0.15$ and $Z = 4629$ m for the surface porosity and compaction depth constant, respectively), and a zero-elevation crustal thickness of 38 km. The flexural isostatic anomaly is based on the T_e distribution in Fig. 9. Note that the Airy isostatic reduction significantly reduces the free-air edge effect high and low and that the flexural isostatic reduction reduces it even further. BMA = Brunswick magnetic anomaly. ECMA = East Coast magnetic anomaly. BSMA = Blake Spur magnetic Anomaly.

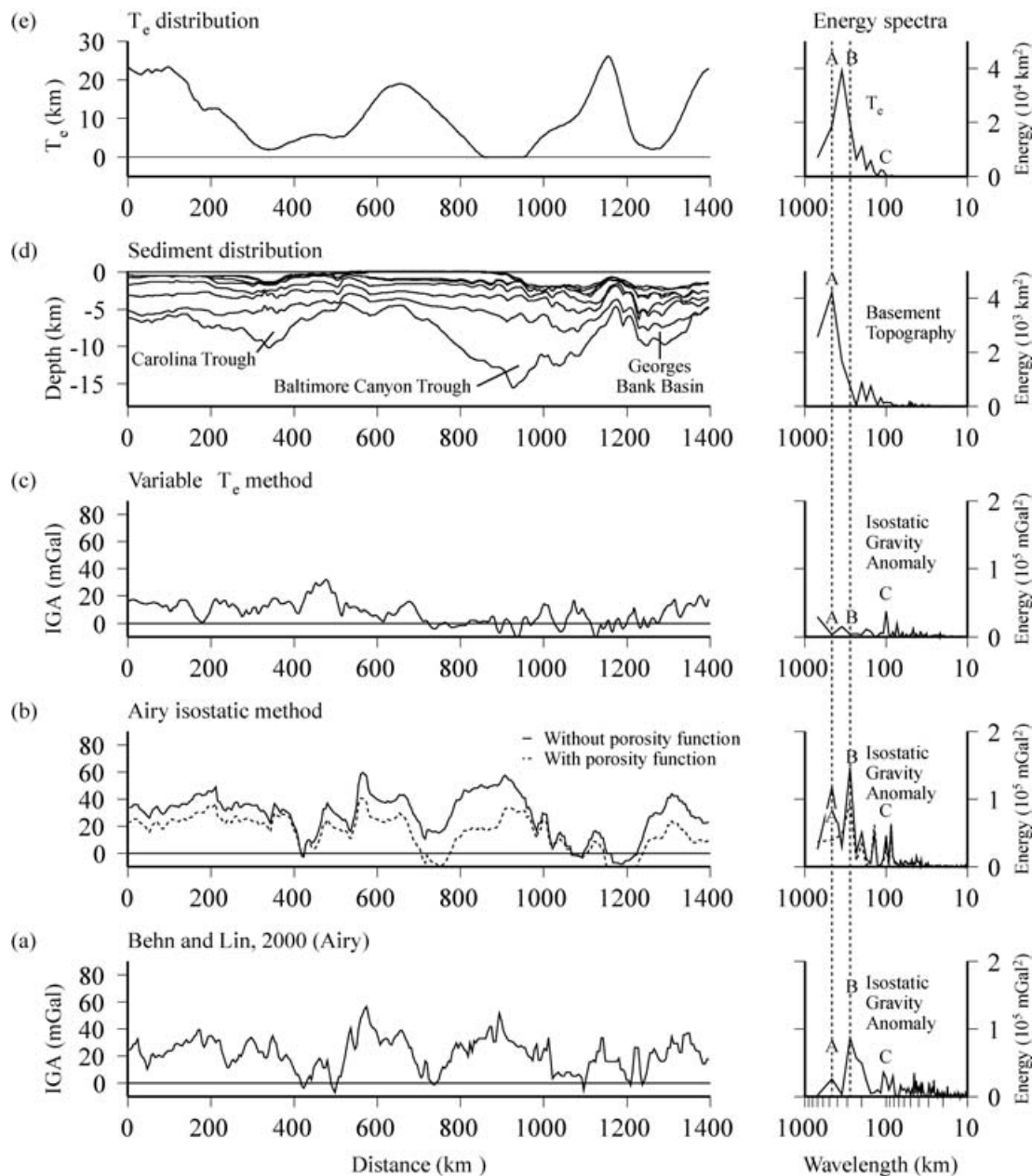


Figure 13. Isostatic gravity anomalies, sediment thickness and T_e distribution along-strike the East Coast, USA margin. The profile follows the crest of the free-air anomaly edge effect high and is located in Fig. 9 (thick solid line). (a) Sediment-corrected Airy isostatic anomaly based on Behn & Lin (2000). (b) Sediment-corrected Airy isostatic anomaly based on the compilation of sediment thickness data in this paper (solid line is without a porosity-depth function, dashed line is with). (c) Sediment-corrected flexural isostatic anomaly based on the T_e distribution in Fig. 9. (d) Sediment distribution. (e) T_e distribution. Note that the flexural isostatic anomaly is a significant improvement on the Airy isostatic anomaly, reducing the amplitude of the anomaly along-strike the margin. The peaks A, B and C on the energy spectra are discussed in the text.

show prominent spectral peaks at wavelengths of ~ 250 km (Peak B) and ~ 500 km (Peak A). Peak A is significantly reduced in the isostatic anomaly based on the Athy porosity versus depth function, suggesting it is related to sediment structure of the margin. The flexural isostatic anomaly, however, shows an absence of *both* Peak A and B. We attribute the absence of Peak B to flexure: the bandwidth of which reflects the T_e structure of the margin.

It is interesting to note from Fig. 13(c) that a prominent spectral peak, C, remains in the flexural isostatic anomaly at wavelengths of ~ 100 km. This is similar to the wavelength identified by Behn & Lin (2000) in both the Airy isostatic and East Coast magnetic anomaly

and attributed by them to segmentation of a slow-spreading ridge. The wavelength corresponds, however, to the cut-off wavelength that we use to band-pass filter the T_e grid and so may, therefore, be a modelling artefact.

Fig. 12(c) shows that flexure does not fully account for the free-air edge effect anomaly along the East Coast, USA margin. The most significant departure is a flexural isostatic anomaly high that characterizes the shelf offshore Virginia and Carolina. The isostatic anomaly high appears to follow the free-air anomaly edge effect high. However, the perspective plots in Fig. 14 clearly show that the free-air edge effect high has a different trend to the flexural isostatic

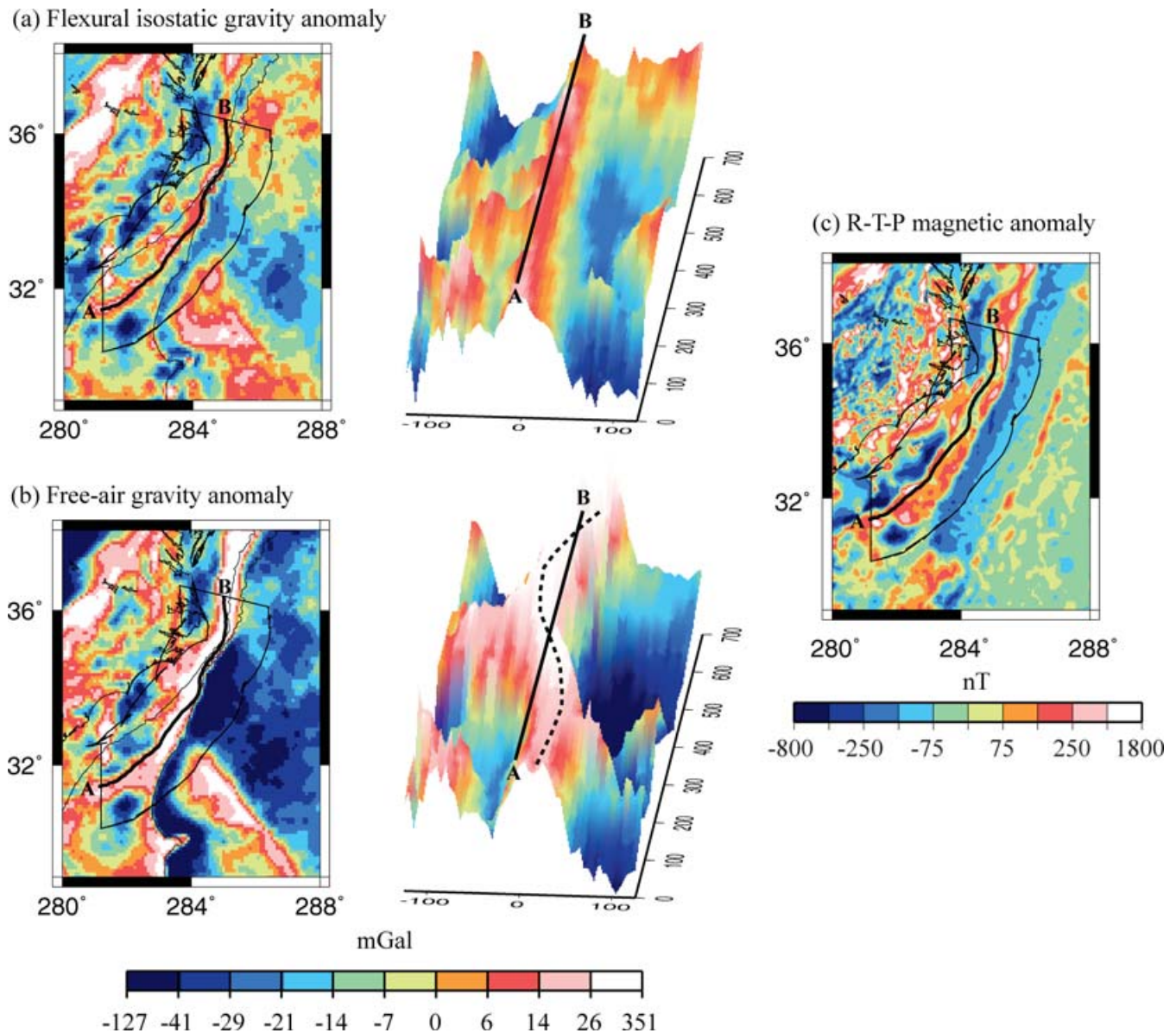


Figure 14. Detailed comparison of the flexural isostatic anomaly (a), free-air anomaly (b), and the Behn & Lin (2000) reduced to the pole magnetic anomaly (c), offshore Virginia, North and South Carolina, and Georgia. The thick solid line shows the location of Profile AB that follows the crest of the flexural isostatic anomaly high. The figure shows that the flexural isostatic anomaly does *not* follow the free-air edge effect high. Rather, the peak in the isostatic anomaly twice crosses the high. The flexural isostatic anomaly high is located just to the west of the ECMA and we attribute it to loading associated with extrusive volcanism and the formation of the SDRs.

anomaly high. This suggests that the combined effects of rifting and sediment loading only account for some of the free-air edge effect anomaly in the region of the shelf break, and therefore, that other processes may have modified this part of the margin during its evolution.

The flexural isostatic anomaly high is flanked by lows, the largest of which is located on the landward side of the high. Together, the isostatic high and flanking low form an arcuate anomaly pattern that extends for some 670 km along-strike the shelf offshore Virginia and Carolina. The peak of the high intersects the EDGE-801, USGS 32 and BA-6 profiles where it correlates with the landward edge of a pattern of SDRs. The SDRs have been interpreted as subaerial volcanic material that formed during the early stages of rifting (Holbrook *et al.* 1994a), suggesting that the isostatic high

and flanking low reflect the response of the crust (and lithosphere) to magmatism.

That this may be the case is suggested in Fig. 14(c) which shows the magnetic anomaly of Verhoef *et al.* (1996), after reduction to the pole by Behn & Lin (2000). The figure shows that the peak of the flexural isostatic anomaly high is parallel to and just to the landward side of the ECMA, which has been interpreted by Behn & Lin (2000) as the result of the juxtaposition of strongly magnetized volcanic material of the SDRs against weakly magnetized continental and Quiet Zone oceanic crust.

In order to test this possibility, we have constructed a crustal model that considers the contribution to the free-air gravity anomaly of rifting, sedimentation, and subaerial volcanism. As Fig. 15 shows, volcanism is associated with a high that is centred over the load and

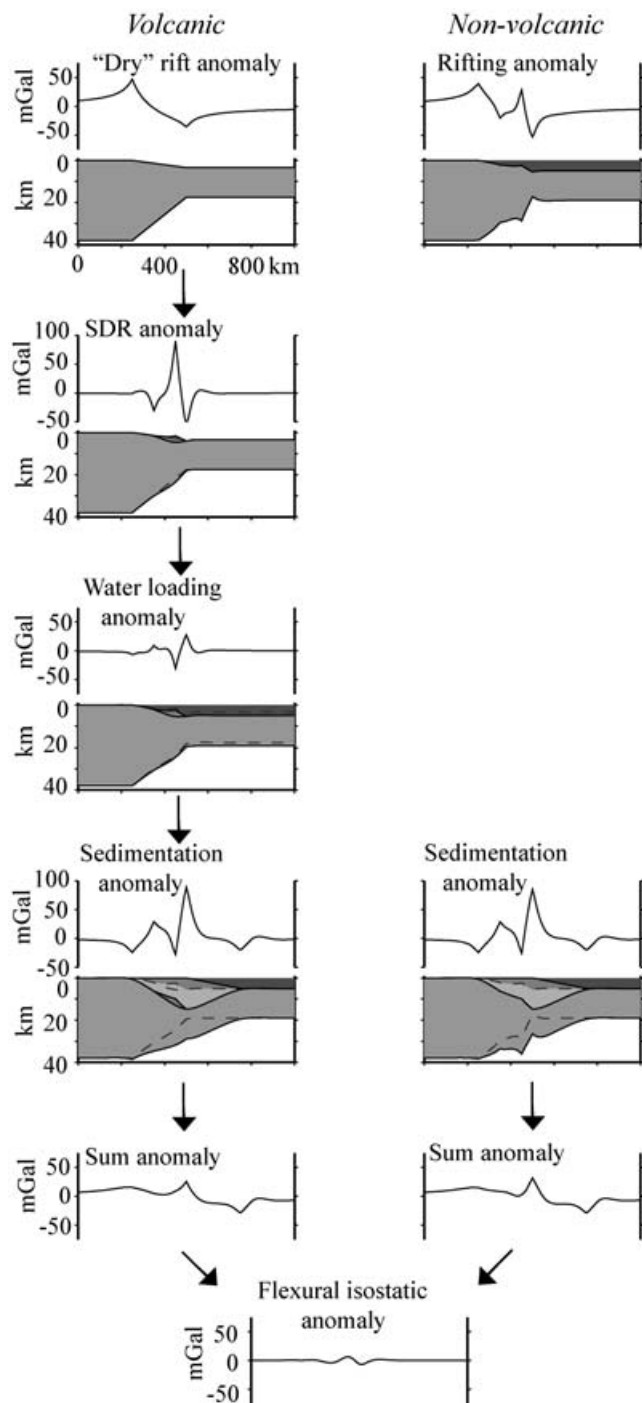


Figure 15. Simple models for the free-air and flexural isostatic gravity anomalies expected for a margin that is characterized by subaerial volcanic, water, and sediment loading. The models are based on densities of 2850, 3330, 1030, 2700, and 2600 kg m⁻³ for the crust, mantle, water, volcanics, and sediments, respectively and a $T_e = 10$ km. (a) The sum gravity anomaly due to 'dry' rifting, subaerial volcanism, flooding and sedimentation. Subaerial volcanism is associated with a high over the load and flanking lows. (b) The sum gravity anomaly that would be expected from sediment backstripping and gravity modelling. (c) The flexural isostatic anomaly associated with the sum anomaly in (a) and (b). The sum anomaly is similar for both cases, but the difference between the two shows a small-amplitude high which corresponds to the subaerial volcanic load and flanking lows. The anomaly pattern closely resembles the anomalies in Fig. 14(b).

flanking lows. The gravity anomaly pattern associated with volcanism is substantially modified by the rifting and sedimentation anomaly and cannot be distinguished in the sum anomaly. However, a high and flanking low are visible in the flexural isostatic anomaly.

As can be seen in Fig. 7, the flexed Moho (i.e. the Moho calculated assuming rifting and sedimentation) along the EDGE-801, USGS 32 and BA-6 profiles is generally shallower in the region of the shelf and slope than the one derived from seismic refraction data. The most likely explanation of this discrepancy is that magmatic material has underplated the base of the flexed crust.

It is perhaps surprising, therefore, that there is apparently little contribution of magmatic underplating to the flexural isostatic gravity anomaly. There is a significant underplating anomaly, for example, at the Hatton Bank (Rockall Bank) margin where the region of the underplate is relatively narrow (<100 km) (Watts & Fairhead 1997). However, the modelling of Wyer (2003) shows that for margins such as the East Coast, USA, where the underplate width may be as large as 300 km, the flexural isostatic anomaly is small, and $\ll 10$ mGal. We speculate, therefore, that the great depth and broad shape of the underplate, together with its relatively low density contrast with surrounding crustal and mantle rocks, has contributed to the underplating anomaly not being more visible at the East Coast, USA margin.

One corollary of these results is that it is difficult, as Behn & Lin (2000) have done, to use the Airy isostatic anomaly to estimate the volume of magmatic material at the East Coast, USA margin. The reasons for this are two-fold. Firstly, a significant portion of the Airy isostatic anomaly, as we have shown, can be attributed to flexure and along-strike and across-strike changes in T_e . Secondly, while the SDRs are associated with a distinct flexural isostatic anomaly, there is little evidence in these anomalies of the associated magmatic underplate.

We note that the arcuate, SDR-correlated, flexural isostatic anomaly is limited to a region of the margin characterized by the Cape Fear and Norfolk arches where the seismic Moho is deeper than the flexed Moho (e.g. Figs 7b–d). The anomaly does not appear to extend to the broad embayments of the Baltimore Canyon Trough and Blake Plateau to the north and south, respectively, where the seismic Moho (at least at the Baltimore Canyon Trough, Fig. 7a) is in better agreement with the flexed Moho. These observations suggest that the East Coast, USA margin maybe segmented along-strike in terms of the volume of both its subaerial volcanism and its associated magmatic underplate. Interestingly, magmatism appears to be focused in a region of the margin where the pre-existing T_e , and hence, long-term mechanical strength is relatively high and the crustal thinning is relatively focused. Therefore, the influence of the inherited flexural strength of the lithosphere on the mode of extension (e.g. wide versus narrow rifts) might extend to magmatic versus amagmatic rifting.

9 CONCLUSIONS

(1) Sediment thickness data have been used together with combined flexural backstripping and gravity modelling techniques to calculate the gravity anomaly associated with rifting and sedimentation anomaly along the East Coast, USA continental margin.

(2) By iteratively comparing the calculated gravity anomalies to the observed free-air gravity anomaly, we have determined the 'best-fit' elastic thickness, T_e , structure of the margin.

(3) We show that $0 < T_e < 40$ km and that T_e varies across-strike and along-strike of the margin.

(4) Since T_e is a proxy for the long-term ($>10^5$ a) integrated strength of the lithosphere, these results imply that the margin is structurally segmented and that weak regions abut strong ones.

(5) T_e generally decreases with increase in the amounts of crustal thinning, β , and the flexed basement curvature, K , suggesting it is controlled, at least in part, by the mechanical structure of the pre-rift lithosphere and yielding due to sediment loading.

(6) However, there is considerable scatter, suggesting other factors such as along-strike changes in crustal composition, geothermal gradient, and strain rate may also contribute.

(7) We show that the spectra of a flexural isostatic anomaly that takes into account the 'best-fit' T_e distribution is significantly reduced in power compared to one which is computed assuming only Airy compensation (i.e. $T_e = 0$ km).

(8) The isostatic anomaly based on the best-fit T_e is not, however, completely subdued. Significant highs and lows persist.

(9) One of the most prominent is an arcuate, 670 km long, high with flanking lows offshore Virginia and Carolina that we attribute to subaerial volcanism during the early stages of continental break-up.

(10) The subaerial volcanism correlates with a region of the margin where lower crustal P -wave velocities are high and the seismic Moho is significantly deeper than the flexed Moho suggesting that magmatic material has been added to the base of the crust. There is, however, little gravity expression of the underplated material.

(11) The arcuate isostatic anomaly terminates to the north at the Baltimore Canyon Trough and to the south at the edge of the Blake Plateau, suggesting that magmatism is segmented along-strike the margin. The origin of the segmentation is not clear, but we attribute it, at least in part, to strength variations in the rifted lithosphere.

ACKNOWLEDGMENTS

We are grateful to Debbie Hutchinson (USGS, Woods Hole) for providing the sediment thickness grid, Marc Behn for providing his Airy isostatic anomaly and magnetic anomaly grids, and Uri ten Brink and Marc Behn for their constructive reviews. The figures were constructed using GMT (Wessel & Smith 1991). This research was supported by a NERC studentship to PW and a NERC/LINK Ocean Margins grant to ABW.

REFERENCES

- Athy, L.F., 1930. Density, porosity and compaction of sedimentary rocks, *Bull. Amer. Assoc. Petrol. Geol.*, **14**, 1–24.
- Behn, M.D. & Lin, J., 2000. Segmentation in gravity and magnetic anomalies along the US East Coast passive margin: implications for incipient structure of the oceanic lithosphere, *J. geophys. Res.*, **105**, 25 769–25 790.
- Braitenberg, C., Wang, Y., Fang, J. & Hsu, H.T., 2003. Spatial variations of flexure parameters over the Tibet-Quinghai plateau, *Earth planet. Sci. Lett.*, **205**, 211–224.
- Brotchie, J.F. & Silvester, R., 1969. On crustal flexure, *J. geophys. Res.*, **74**, 5240–5245.
- Brown, P.M., Miller, J.A. & Swain, F.M., 1972. Structural and stratigraphic framework, and spatial distribution of permeability of the Atlantic coastal plain, North Carolina to New York, *US Geological Survey Prof. Paper*, **796**, 1–79.
- Burov, E.B. & Diament, M., 1995. The effective elastic thickness (T_e) of continental lithosphere: what does it really mean?, *J. geophys. Res.*, **100**, 3895–3904.
- Burov, E. & Poliakov, A., 2001. Erosion and rheology controls on synrift and postrift evolution: Verifying old and new ideas using a fully coupled numerical model, *J. geophys. Res.*, **106**, 16 461–16 481.
- Chand, S. & Subrahmanyam, C., 2003. Rifting between India and Madagascar—mechanism and isostasy, *Earth planet. Sci. Lett.*, **210**, 317–332.
- Childs, O.E. & Salvador, A., 1985. Correlation of stratigraphic units of North America (COSUNA), *Amer. Assoc. Pet. Geol.*, **89**, 7861–7876.
- Erickson, S.G., 1993. Sedimentary loading, lithospheric flexure, and subduction initiation at passive margins, *Geology*, **21**, 125–128.
- Gahli, A. & Neville, A.M., 1989. *Structural analysis: A unified classical and matrix approach*, Chapman and Hall, London.
- Goetze, C. & Evans, B., 1979. Stress and temperature in the bending lithosphere as constrained by experimental rock mechanics, *Geophys. J. R. astr. Soc.*, **59**, 463–478.
- Grow, J.A., 1981. Structure of the Atlantic Margin of the United States, in *Geology of Passive Continental Margins*, pp. 3-1–3-41, ed. Bally, A.W., Amer. Assoc. Pet. Geol., Tulsa, Oklahoma.
- Gunn, R., 1944. A quantitative study of the lithosphere and gravity anomalies along the Atlantic coast., *Franklin Inst. J.*, **237**, 139–154.
- Holbrook, W.S. & Kelemen, P.B., 1993. Large Igneous Province on the US Atlantic Margin and implications for magmatism during continental breakup, *Nature*, **364**, 433–436.
- Holbrook, W.S., Purdy, G.M., Sheridan, R.E., III, L.G., Talwani, M., Ewing, J. & Hutchinson, D., 1994a. Seismic structure of the U.S. mid-Atlantic continental margin, *J. geophys. Res.*, **99**, 17 871–17 891.
- Holbrook, W.S., Reiter, E.C., Purdy, G.M., Sawyer, D., Stoffa, P.L., Austin, J.A., Oh, J. & Makris, J., 1994b. Deep structure of the US Atlantic continental margin offshore South Carolina from coincident ocean bottom and multichannel seismic data, *J. geophys. Res.*, **99**, 9155–9178.
- Hutchinson, D., Klitgord, K.D. & Detrick, R.S., 1986. Rift basins of the Long Island Platform, *Geol. Soc. Am. Bull.*, **97**, 688–702.
- Hutchinson, D.R., Poag, C.W. & Popenoe, P., 1996. Geophysical database of the East Coast, of the United States: southern Atlantic Margin-Stratigraphy and velocity from multichannel seismic profiles, *US Geol. Survey Open File Report*, 95-27, 65.
- Jordan, T.A. & Watts, A.B., 2005. Gravity anomalies, flexure and the elastic thickness structure of the India-Eurasia collisional system. *Earth. Planet. Sci. Letts*, **236**, 732–750.
- Karner, G.D. & Watts, A.B., 1982. On isostasy at Atlantic-type continental margins, *J. geophys. Res.*, **87**, 2923–2948.
- Keen, C.E. & Dehler, S.A., 1997. Extensional styles and gravity anomalies at rifted continental margins: some North Atlantic examples, *Tectonics*, **16**, 744–754.
- Keen, C.E., Keen, M.J., Barrett, D.L. & Heffler, D.G., 1975. Some aspects of the ocean-continent transition at the continental margin of eastern North America, in *Offshore Geology of eastern Canada*, pp. 189–197, Geol. Surv. Canada.
- Klitgord, K.D., Poag, C.W., Schneider, C.M. & North, L., 1994. Geophysical database of the east Coast of the United States northern Atlantic continental margin: cross sections and gridded database (Georges Bank basin, Long Island platform, and Baltimore Canyon trough), *US Geol. Survey Open-File Report*, 94-637, 187.
- Klitgord, K.D., Hutchinson, D.R. & Schouten, H., 1988. US Atlantic continental margin: Structural and tectonic framework, in *The Atlantic Continental Margin*, pp. 19–56, eds Sheridan, R.E. & Grow, J.A., Geological Society of America, Boulder, Colorado.
- Kooi, H., Cloetingh, S. & Burrus, J., 1992. Lithospheric necking and regional isostasy at extensional basins I. Subsidence and gravity modeling with an Application to the Gulf of Lions Margin (SE France), *J. geophys. Res.*, **97**, 17 553–17 571.
- Krishna, M.R., Chand, S. & Subrahmanyam, C., 2000. Gravity anomalies, sediment loading and lithospheric flexure associated with the Krishna-Godavari basin, eastern continental margin of India, *Earth planet. Sci. Lett.*, **175**, 223–232.
- Kruse, S.E. & Royden, L.H., 1994. Bending and unbending of an elastic lithosphere: the Cenozoic history of the Apennine and Dinaride foredeep basins, *Tectonics*, **13**, 278–302.
- LASE study group, 1986. The Structure of the US East Coast Passive Margin from Large Aperture Seismic Experiments (LASE), *Marine Petrol. Geol.*, **3**, 234–242.

- Laske, G. & Masters, G., 1997. A global digital map of sediment thickness, *EOS, Trans. Am. geophys. Un.*, **78**, F483.
- Lin, A.T. & Watts, A.B., 2002. Origin of the West Taiwan basin by orogenic loading and flexure of a rifted continental margin, *J. geophys. Res.*, **107**, doi:10.1029/2001JB000669.
- Manspeizer, W., 1985. Early Mesozoic History of the Atlantic Passive Margin, in *Geologic Evolution of the United States Atlantic margin*, edited by Poag, C.W., pp. 1–24, Van Nostrand Reinhold Company, New York.
- Marzoli, A., Renne, P.R., Piccirillo, E.M., Ernesto, M., Bellieni, G. & Min, A.D., 1999. Extensive 200-million-year-old continental flood basalts of the central Atlantic magmatic province, *Science*, **284**, 616–618.
- McHone, J.G., 2000. Non-plume magmatism and tectonics during the opening of the central Atlantic ocean, *Tectonophysics*, **316**, 287–296.
- McKenzie, D.P., 1978. Some remarks on the development of sedimentary basins, *Earth planet. Sci. Lett.*, **40**, 25–32.
- McNutt, M.K. & Menard, H.W., 1982. Constraints on yield strength in the oceanic lithosphere derived from observations of flexure, *Geophys. J. R. astr. Soc.*, **71**, 363–394.
- Mountain, G.S. & Tucholke, B.E., 1985. Mesozoic and Cenozoic geology of the U.S. Atlantic continental slope and rise, in *Geologic evolution of the United States Atlantic Margin*, pp. 293–341, ed. Poag, C.W., Van Nostrand Reinhold, New York.
- Muller, R.D., Roest, W.R., J.-Y. Royer, Gahagan, L.M. & Sclater, J.G., 1997. Digital isochrons of the world's ocean floor, *J. geophys. Res.*, **102**, 3211–3214.
- Noltimier, H.C., Fidler, M.L. & Loveday, D.C., 2004. New view of segment of the east continent rift basin, Ohio based on gravity, geomagnetic, and seismic surveys, *Geol. Soc. Am. Abstracts, 2004 Denver Annual Meeting*, Paper 213-10.
- Owens, J.P. & Gohn, G.S., 1985. Depositional history of the Cretaceous series in the U.S. Atlantic coastal plain: stratigraphy, paleoenvironments, and tectonic controls of sedimentation., in *Geologic evolution of the United States Atlantic margin*, pp. 25–86, ed. Poag, C.W., Van Nostrand Reinhold Company, New York.
- Parker, R.L., 1972. The rapid calculation of potential anomalies, *Geophys. J. R. astr. Soc.*, **31**, 447–455.
- Pazzaglia, F.J. & Gardner, T.W., 1994. Late Cenozoic flexural deformation of the middle U.S. Atlantic passive margin, *J. geophys. Res.*, **99**, 12 143–12 157.
- Rabinowitz, P.D. & LaBreque, J., 1979. The Mesozoic South Atlantic Ocean and Evolution of its Continental Margins, *J. geophys. Res.*, **84**, 5973–6002.
- Rapp, R.H. & Pavlis, N.K., 1990. The development and analysis of geopotential coefficient models to spherical harmonic degree 360, *J. geophys. Res.*, **95**, 21 885–21 911.
- Sandwell, D.T. & Smith, W.H.F., 1997. Marine gravity anomaly from Geosat and ERS-1 satellite altimetry, *J. geophys. Res.*, **102**, 10 039–10 054.
- Schlee, J.S., 1981. Seismic stratigraphy of Baltimore Canyon Trough, *Am. Assoc. Pet. Geol. Bull.*, **65**, 26–53.
- Schlee, J., Behrendt, J.C., Grow, J.A., Robb, J.M., Maattick, R.E., Taylor, P.T. & Lawson, B.A., 1976. Regional Geologic Framework off Northeastern United States, *Amer. Assoc. Pet. Geol. Bull.*, **60**, 926–951.
- Sempere, J.C., Purdy, G.M. & Schouten, H., 1990. Segmentation of the Mid-Atlantic Ridge between 24°N and 30°40'N, *Nature*, **344**, 427–431.
- Sheridan, R.E. et al., 1993. Deep seismic reflection data of EDGE US mid-Atlantic continental margin experiment: implications for Appalachian sutures and Mesozoic rifting and magmatic underplating, *Geology*, **21**, 563–567.
- Steckler, M.S. & Watts, A.B., 1978. Subsidence of the Atlantic-type continental margin off New York, *Earth planet. Sci. Lett.*, **41**, 1–13.
- Stewart, J. & Watts, A.B., 1997. Gravity anomalies and spatial variations of flexural rigidity at mountain ranges, *J. geophys. Res.*, **102**, 5327–5352.
- Stewart, J., Watts, A.B. & Bagguley, J., 2000. Three-dimensional subsidence analysis and gravity modelling of the continental margin offshore Namibia, *Geophys. J. Int.*, **141**, 724–746.
- Talwani, M. & Eldholm, O., 1973. The boundary between continental and oceanic crust at the margin of rifted continents, *Nature*, **241**, 325–330.
- Thomas, W.A., 2006. Tectonic inheritance at a continental margin, *GSA Today*, **16**, 4–11.
- Timoshenko, S.P. & Woinowsky-Krieger, S., 1959. *Theory of Plates and Shells*, McGraw-Hill, New York.
- Trehu, A.M., Ballard, A., Dorman, L.M., Gettrust, J.F., Klitgord, K.D. & Shreiner, A., 1989. Structure of the lower crust beneath the Carolina trough, US Atlantic continental margin, *J. geophys. Res.*, **94**, 10 585–10 600.
- Van Wees, J.D. & Cloetingh, S., 1994. A finite-difference technique to incorporate spatial variations in rigidity and planar faults into 3-D models for lithospheric flexure, *Geophys. J. Int.*, **117**, 179–195.
- Verhoef, J., Roest, W.R., Macnab, R. & Arkani-Hamed, J., 1996. Magnetic anomalies of the Arctic and North Atlantic Oceans and adjacent land areas, *Geol. Surv. Can.*, Open File Rep. 3125.
- Walcott, R.I., 1972. Gravity, flexure, and the growth of sedimentary basins at a continental edge, *Geol. soc. Am. Bull.*, **83**, 1845–1848.
- Wang, Y. & Mareschal, J.-C., 1999. Elastic thickness of the lithosphere in the Central Canadian Shield, *Geophys. Res. Lett.*, **26**, 3033–3036.
- Watts, A.B., 1978. An analysis of isostasy in the world's oceans:1. Hawaiian-Emperor Seamount Chain, *J. geophys. Res.*, **83**, 5989–6004.
- Watts, A.B., 1988. Gravity anomalies, crustal structure and flexure of the lithosphere at the Baltimore Canyon Trough, *Earth planet. Sci. Lett.*, **89**, 221–238.
- Watts, A.B., 2001a. Gravity anomalies, flexure and crustal structure at the Mozambique rifted margin, *Mar. and Pet. Geol.*, **18**, 445–455.
- Watts, A.B., 2001b. *Isostasy and flexure of the lithosphere*, 458 pp., Cambridge University Press, Cambridge.
- Watts, A.B. & Burov, E.B., 2003. Lithospheric strength and its relationship to the elastic and seismogenic thickness, *Earth planet. Sci. Lett.*, **213**, 113–131.
- Watts, A.B. & Fairhead, J.D., 1997. Gravity anomalies and magmatism at the British Isles continental margin, *J. Geol. Soc. Lond.*, **154**, 523–529.
- Watts, A.B. & Marr, C., 1995. Gravity anomalies and the thermal and mechanical structure of rifted continental margins, in *Rifted Ocean-Continent Boundaries*, pp. 65–94, eds Banda, E., Talwani, M. & Torné, M., Kluwer Academic Publishers, Dordrecht.
- Watts, A.B. & Stewart, J., 1998. Gravity anomalies and segmentation of the continental margin offshore West Africa, *Earth planet. Sci. Lett.*, **156**, 239–252.
- Watts, A.B. & Zhong, S., 2000. Observations of flexure and the rheology of oceanic lithosphere, *Geophys. J. Int.*, **142**, 855–875.
- Weissel, J.K. & Karner, G.D., 1989. Flexural uplift of rift flanks due to mechanical unloading of the lithosphere during extension, *J. geophys. Res.*, **94**, 13 919–13 950.
- Wessel, P. & Smith, W.H.F., 1991. Free software helps map and display data, *EOS, Trans. Am. geophys. Un.*, **72**, 441–446.
- Worzel, J.L., 1965. Deep Structure of Coastal Margins and Mid-Oceanic Ridges, in *Submarine Geology and Geophysics*, pp. 335–361, eds Whittard, W.F. & Bradshaw, R., Butterworths, London.
- Wyer, P., 2003. Gravity anomalies and segmentation of the eastern USA passive continental margin, *PhD thesis*, Oxford.